Bulletin of Volcanology (2022) 84: 93
https://doi.org/10.1007/s00445-022-01601-4

RESEARCH ARTICLE

Eruptive history of Mason Spur, a Miocene—Pleistocene polygenetic volcanic complex in southern Victoria Land, West Antarctic Rift System, Antarctica

John L. Smellie[1] · Adam P. Martin[2] · Gianfranco Di Vincenzo[3] · Dougal B. Townsend[4] · Matthew T. Heizler[5] · Dawn C. S. Ruth[5,6]

Received: 23 June 2022 / Accepted: 5 September 2022 / Published online: 19 September 2022

Abstract

Mason Spur is a deeply eroded Middle Miocene to Pleistocene (c. 13 to 0.37 Ma) volcanic complex in southern Victoria Land, within the West Antarctic Rift System (WARS). The oldest rocks include a large volume of trachyte ignimbrites that provided abundant volcanic detritus recovered in McMurdo Sound drill cores. The ignimbrites together with early-formed intrusions were strongly deformed during a substantial caldera collapse at c. 13 Ma. Intense erosion modified the volcanic landscape, creating a paleo-relief of several hundred metres. Deep ravines were cut and filled by deposits of multiple lahars probably linked to gravitational collapses of trachyte dome(s). Small-volume trachytic magmas were also erupted, forming lavas and at least one tuff cone. The youngest trachytic activity comprises a lava dome and related block-and-ash-flow deposits, erupted at 6 Ma. Basanite erupted throughout the history of the complex and eruptions younger than 12 Ma are almost exclusively basanite, forming scoria cones, water-cooled lavas, and tuff cones. Three peripheral outcrops are composed of basanitic ‘a‘ā lava-fed deltas, probably erupted from vents on neighbouring volcanoes at Mount Discovery and Mount Morning. Abundant ignimbrite deposits at Mason Spur differentiate this volcanic complex from others in the WARS. Eruptions were triggered by rift extension initially, yielding the voluminous trachytes sourced from a magma chamber on the margin of the WARS. Later mafic eruptions were associated with deep crustal faults related to residual intraplate deformation. These results add important details to the eruptive history of the intracontinental WARS.

Keywords Caldera · Ignimbrite · Dome · Block-and-ash-flow · Lahar · ‘a ‘ā lava-fed delta

Introduction

Antarctica hosts one of Earth’s largest intracontinental rift provinces, the West Antarctic Rift System (WARS), which contains numerous large polygenetic volcanoes (Wilch et al. 2021; Fig. 1). They have a range of ages spanning the past 37 Myr but most are Middle Miocene and younger (≤ 14 Ma) and the volcanism is still active at prominent centres such as Mount Erebus, Mount Berlin, and Mount Melbourne (Geyer 2021). Antarctica is also covered by Earth’s largest ice sheet and most of the volcanoes inland are largely obscured by ice. The Antarctic ice sheet has had a predominantly cold-based thermal regime since c. 14 Ma (Lewis et al. 2007) and, with rare exception (e.g., Crary Mountains and Mount Sidley, Marie Byrd Land; Panter et al. 1994; Wilch and McIntosh 2002), volcanoes that are exposed above the present-day ice have undergone only minimal erosion (Rocchi et al. 2006). Thus, their volcanic evolution is very poorly known. By

Editorial responsibility: M.H. Ort; Deputy Executive Editor: L. Pioli

✉ John L. Smellie
jls55@le.ac.uk

[1] School of Geography, Geology and the Environment, University of Leicester, Leicester LE1 7RH, UK

[2] GNS Science, Private Bag 1930, Dunedin, New Zealand

[3] Istituto di Geoscienze e Georisorse, Consiglio Nazionale Delle Ricerche, I-56127 Pisa, Italy

[4] GNS Science, PO Box 30-368, Lower Hutt, New Zealand

[5] New Mexico Bureau of Geology and Mineral Resources, Socorro, NM 87801, USA

[6] US Geological Survey, Menlo Park, CA 94025, USA

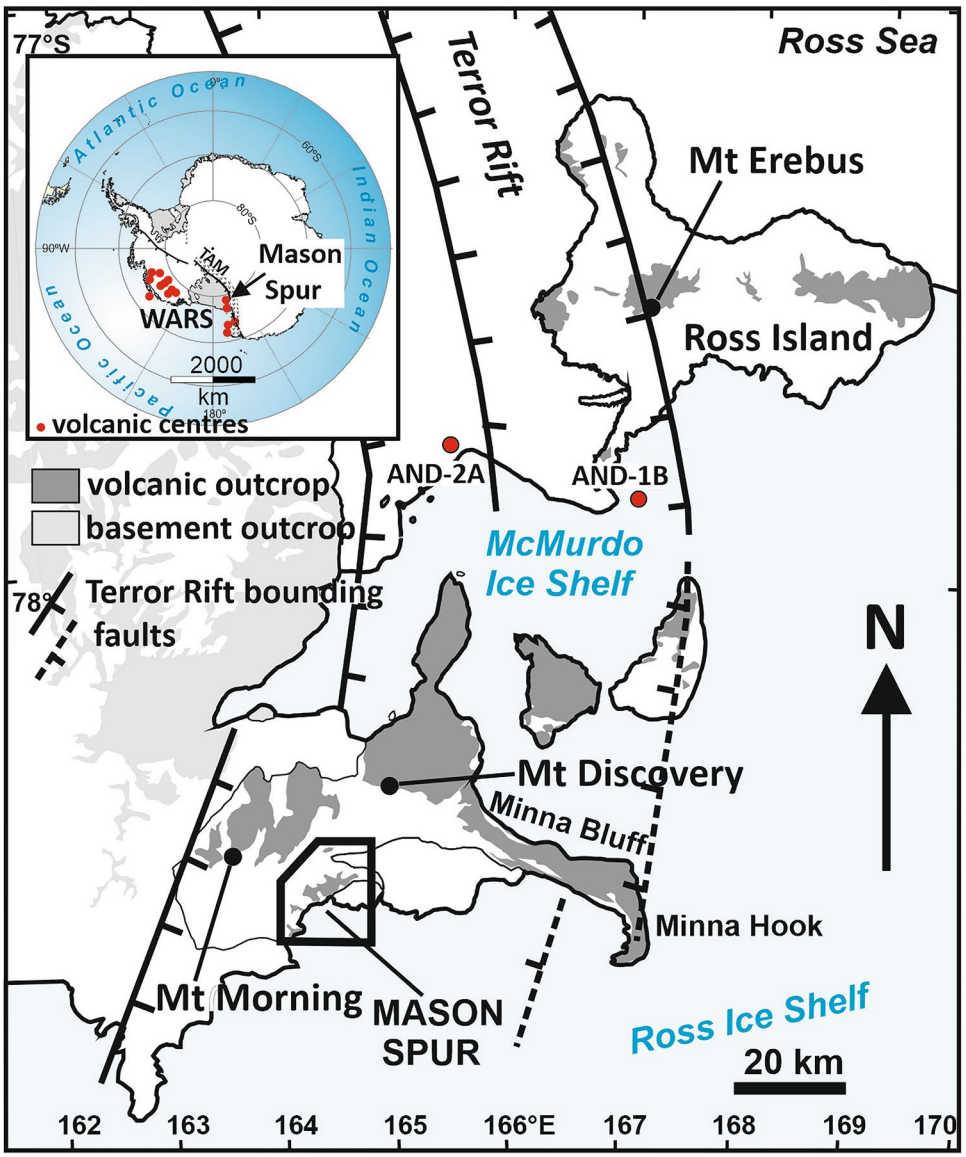

Fig. 1 Map showing the location of Mason Spur within the Erebus Volcanic Province and the West Antarctic Rift System (WARS; inset, with selected large volcanoes shown as red dots). Possible bounding fractures of the Terror Rift are also shown (from Horgan et al. 2005), as are the locations of two drillsites, AND-1B and AND-2A. The field area described in this paper is outlined by a black polygon. TAM—transantarctic mountains (stippled ornament)

contrast, volcanoes within the WARS that are situated in coastal areas have frequently undergone extensive erosion, mainly marine, during interglacial periods (Smellie 2021). This has resulted in several volcanoes being exposed deep into their interiors, for example in northern Victoria Land and eastern Marie Byrd Land (LeMasurier et al. 1994; Wilch and McIntosh 2002; Smellie et al. 2011a).

This paper describes the geology and volcanic evolution of Mason Spur, a prominent south-east-facing volcanic massif 1300 m high and c. 14 km in length that overlooks a deep embayment in the Ross Ice Shelf, southern Victoria Land (Fig. 2). It is situated below the south-east flank of the large mainly Plio-Pleistocene Mount Morning volcano (< 5 Ma; though ages as old as 25 Ma are inferred; Martin et al. 2010; Fig. 1). Mason Spur has been extensively and deeply eroded because of its coastal location and age, resulting in > 1000 m of relief and significant exposure of the deep stratigraphy. The locality has been visited rarely and the previous studies focussed on the age, geochemistry and petrological evolution of the basanite—trachyte magmatic lineages present (Wright-Grassham 1987; Martin et al. 2010, 2013, 2021a, b). However, those studies described an unusually wide variety of volcanic products, including lava flows, a lava dome, scoria cones, hyaloclastite, pillow lava, volcanic breccia, tuff cones, tuff rings, lahar and fluvial deposits, and diamictite.

In this paper, we review the volcanic evolution of the long-lived Mason Spur volcanic complex using stratigraphical studies and a new geological map (Fig. 3). Because of the excellent exposure, the outcrops provide a rare opportunity to document the geological history and evolution of one of the large WARS volcanic centres. Twenty-one new $^{40}Ar/^{39}Ar$ dates give an improved eruptive chronology and allow a

Fig. 2 View of Mason Spur looking north-east from 'Helms Deep' (Dunbar Head; see Fig. 3 (inset) for location). The base of the crag is mostly above c. 400 m above sea level and the summit is at c. 1300 m. It has been exposed by a combination of glacial and marine erosion

comprehensive reassessment of the volcanic evolution to be made. An important result of our study is the discovery of a thick caldera-filling sequence of ignimbrites, reported initially by Martin et al. (2018). Similar deposits are very rare and much less voluminous elsewhere in the WARS and our study thus fills a significant gap in our knowledge of the eruptive and structural evolution of the large polygenetic WARS volcanoes.

Geological background

Mason Spur is situated in southern Victoria Land within the WARS, which measures 500–700 km in width, over 3000 km in length and covers an area of c. 1.2×10^6 km^2 (Fig. 1, inset; LeMasurier 2008; Jordan et al. 2020). The large volcanoes in southern Victoria Land are included in the Erebus Volcanic Province of the McMurdo Volcanic Group. They include Mount Erebus, Mount Bird, Mount Terror, Mount Discovery, and Mount Morning (Fig. 1; Smellie and Martin 2021). Mason Spur represents one of the early stages of volcanism of the Mount Morning Volcanic Field. Previous geological studies of Mason Spur were a PhD project by Wright-Grassham (1987; a brief summary is given by Wright and Kyle 1990) and papers by Martin et al. (2010, 2013, 2018). The study by Wright-Grassham (1987) was reconnaissance in nature and investigated Mount Discovery, Mount Morning and Minna Bluff in addition to Mason Spur. Martin et al. (2010, 2013) examined the petrology of Mount Morning and undertook isotopic dating but they included a brief study of Mason Spur. Wright-Grassham (1987) informally defined the "Mason volcanic complex," a name that we also adopt in this paper, and identified two petrological suites: an older suite ranging from mugearite to peralkaline trachyte and a younger suite of mainly basanites/tephrites and benmoreites (also Martin et al. 2010, 2013, 2021a, b). Helms Bluff, situated 5 km north of Mason Spur (Fig. 3), is also included in our study for completeness since it was previously regarded as part of the Mason Spur sequence (Wright-Grassham 1987). However, on the basis of transport directions for the volcanic units present (lava-fed deltas; see later) and an isotopic age that is younger than volcanic units at Mason Spur apart from late-stage scoria cones, it is regarded as an outlier of the neighbouring Mount Discovery volcano (see Smellie and Martin 2021, and below).

The lithological descriptions of Mason Spur by Wright-Grassham (1987) include references to numerous sedimentary and volcaniclastic units. However, the study by Wright-Grassham (1987) is now 35 years old and, given the more focused nature of our study and numerous significant advances in volcanology that have taken place since the initial study, we provide a new stratigraphy and geological interpretation.

Methods and terminology

For this study, fieldwork by JS, AM, and DT at Mason Spur occurred over 21 days during January 2017. It built on 10 days of fieldwork by AM in 2005. Outlying areas near Dunbar Head, and at Helms Bluff and Snow Petrel Peak were accessed during short visits by helicopter. A new and significantly revised lithostratigraphical geological map is presented in Fig. 3. Rock samples were taken for petrography and isotopic dating. More than seventy thin sections were examined and 21 geochronology

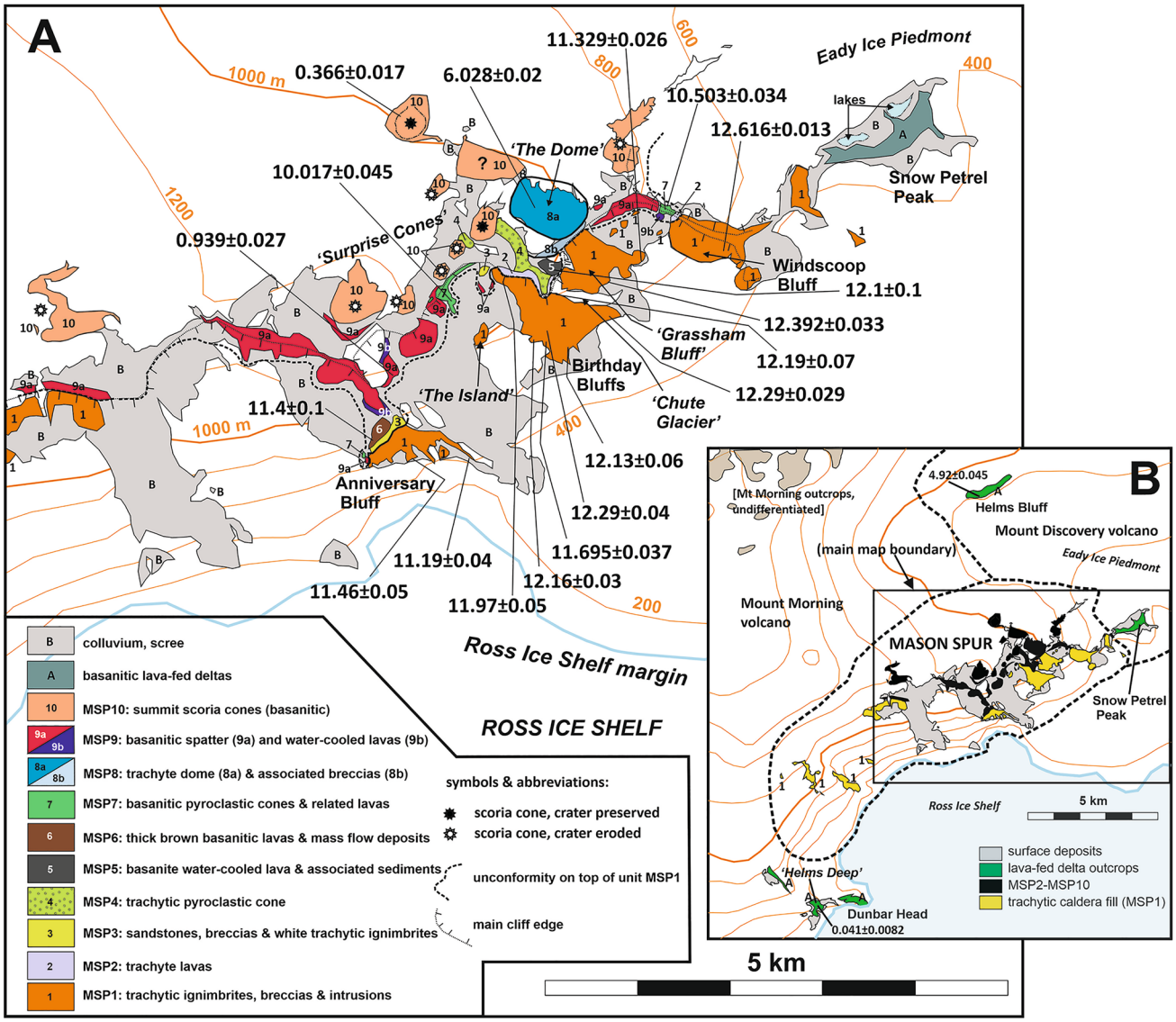

Fig. 3 (A) Geological map of Mason Spur showing the distribution of mapped units (MSP1-MSP10) and the locations and ages of samples dated during this investigation (ages reported in Ma; errors are 2σ). (B) Map of Mason Spur and surrounding area showing the inferred boundaries of the major volcanoes and the Mason Spur volcanic complex (dashed lines), simplified geology, and the locations and ages of outlying outcrops discussed in this paper

samples analyzed. The isotopic dating was carried out at the Istituto di Geoscienze e Georisorse, Consiglio Nazionale delle Ricerche (Pisa, Italy) and at the New Mexico Geochronology Research Laboratory (USA). A full description of the dating results and methods used is presented in Supplementary Information S1. A summary of the petrology of Mason Spur is presented by Martin et al. (2021a, b) and representative major oxide compositions are provided in Supplementary Information S2. Elevations and unit thicknesses were determined by hand-held GPS (Garmin eTrex), adjusted for daily pressure drift and calibrated to fixed locations in the field, with an estimated error of ± 10 m.

"Ignimbrite" is used to denote any pumiceous ash-rich deposit laid down by the wide spectrum of pyroclastic density currents, ranging from fully dilute to concentrated (granular fluid-based), following the recommendations of Branney and Kokelaar (2002; also Giordano and Cas 2021). The terminology for other volcaniclastic rocks follows that of White and Houghton (2006), and rock compositional names are after Le Maitre et al. (2002). Unofficial place names used are indicated by inverted commas at first use in the text and on maps.

Stratigraphy of the Mason Spur volcanic complex

A schematic cross section of Mason Spur illustrating the lithostratigraphy proposed in this study and the vertical and lateral relationships is shown in Fig. 4. Details of the stratigraphical units are given in Tables 1 and 2 and representative images of the lithofacies in Figs. 5, 7, and 8. Full descriptions of the lithofacies are presented in Supplementary Information S3, and additional supporting images are presented in Supplementary Information S4 and S5 to give a comprehensive view of the geology.

The lithostratigraphical units are designated MSP1-MSP10, which distinguishes them from the older terminology of Wright-Grassham (1987; Table 1). There are some similarities between our units and those mapped by Wright-Grassham (1987). However, a major difference with our study is that units MS1–MS5 of Wright-Grassham (1987) appear to have little basis for separate lithostratigraphical distinction. They mainly correspond to variations in the proportions of trachytic ignimbrites, breccias, and hypabyssal intrusions that are grouped together in our unit MSP1 (Fig. 5a–e). MSP1 is chaotic and many hundreds of metres thick. It is overlain unconformably by trachytic lavas (MSP2), volcano-sedimentary units (MSP3 [trachytic; Figs. 6a, b and 7], and MSP6 [basanitic; Fig. 7]), a trachyte pyroclastic cone (MSP4; Fig. 6c), water-cooled basanite lava and interbedded sedimentary rocks (MSP5), a trachyte dome (MSP8; Fig. 6e, f, g), and basanite pyroclastic cones, lavas and scoria deposits (MSP7, MSP9, MSP10; Figs. 6d, 8a–d). Additionally, outlying outcrops at "Helms Deep," Snow Petrel Peak and Helms Bluff (Fig. 3b) are mafic lava-fed deltas sourced from nearby volcanoes (Fig. 8e, f). The delta outcrops are not linked genetically to eruptions at Mason Spur (see later), and collectively they are not given an MSP stratigraphical designation.

Unlike most other volcanoes within the WARS (Smellie 2021; Wilch et al. 2021), the stratigraphy at Mason Spur is dominated by clastic units, varying from ignimbrites, scoria, and agglutinate to sandstones and breccio-conglomerates, but lavas and intrusions are also locally prominent. The bulk of the outcrop is dominated by ignimbrite and breccia deposits and hypabyssal intrusions of MSP1. It has a minimum thickness of 800 m. Subsequent units are volumetrically

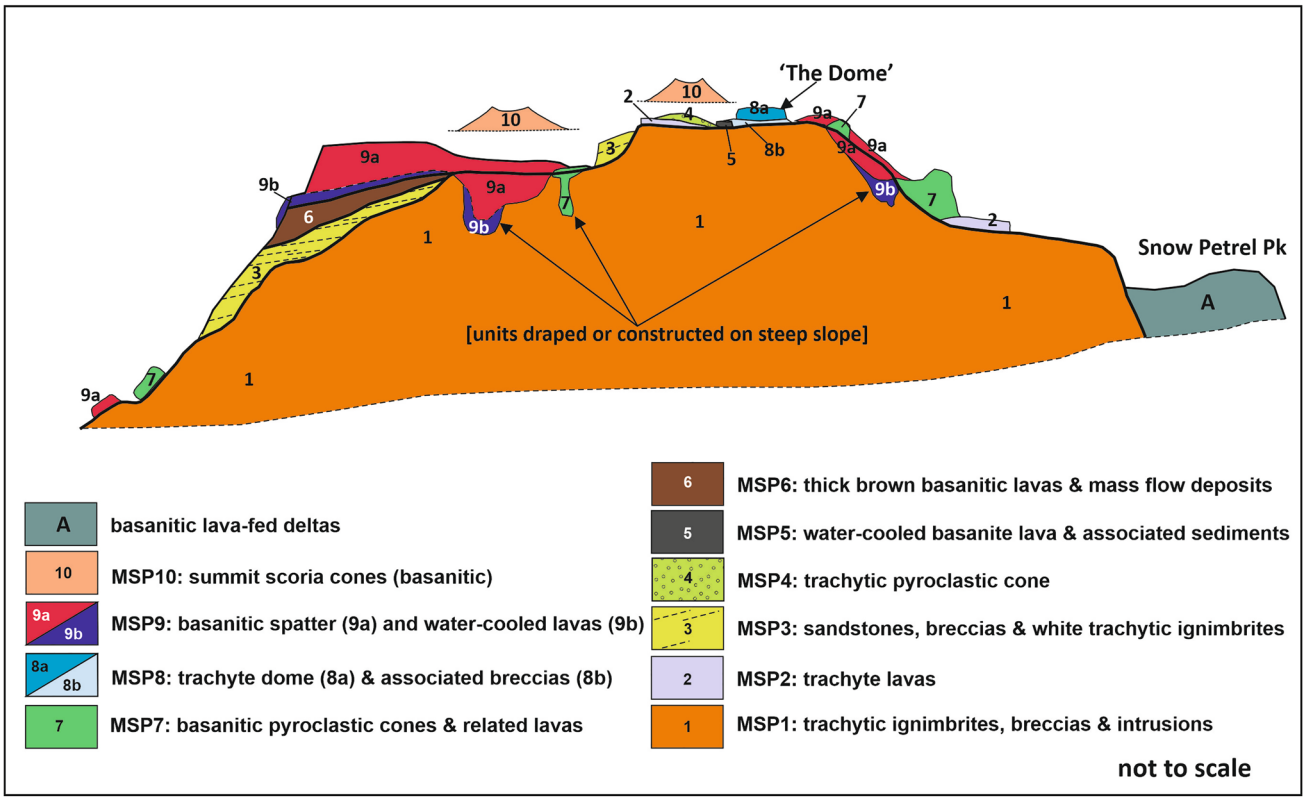

Fig. 4 Schematic west south-west—east north-east cross section of Mason Spur (not to scale) showing the relationships between the different lithostratigraphical units identified in this study. Some of the units crop out on the modern slope or above and behind the section but they are included in the sketch where indicated. Note how unit MSP1 has been severely eroded prior to the deposition of younger units, with > 800 m of relief present. The eroded upper surface of MSP1 has a topographical relief of several hundred meters

Table 1 Lithostratigraphy and summary characteristics of stratigraphical units at Mason Spur

Stratigraphical unit**	Distinguishing characteristics	Composition***	Description	Comments
[un-numbered]	lava—breccia couplets	basanite	'A'ā lavas & rare pāhoehoe lavas, not accessed, largely eroded; overlie massive chaotic breccia deposits with numerous water-cooled lava lobes; deposits individually > 200–270 m thick	Outcrops at 'Helms Deep', Helms Bluff and Snow Petrel Peak; sourced from outside of Mason Spur volcano
MSP10	summit scoria cones	basanite	Several scoria cones up to 800 m in diameter composed of maroon scoria, agglutinate & clastogenic lavas	Includes 'Surprise Cones', a linear row of degraded small (< 150 m wide) scoria cones that extends SW of 'The Dome'
MSP9	spatter and water-cooled lavas	basanite	Agglutinate and clastogenic lavas (Fig. 8a; MSP9a); maximum thickness c. 80–100 m in the crags NNW of Anniversary Bluff; locally underlain by water-cooled lavas (MSP9b); only MSP9a occurs at lower elevations (MSP9b absent). MSP9a lavas have maroon scoriaceous autobreccias. MSP9b lavas dark grey, fine grained to aphanitic with well-developed blocky, pseudopillow and weak prismatic jointing (Fig. 8b); rare glassy clasts in associated fines-poor breccia	Strongly eroded outcrops with no primary volcanic landforms. Lavas throughout unit MSP9 petrologically similar and likely coeval
MSP8	dome and dome breccias	trachyte	Almost circular dome-like outcrop c. 900 m in diameter (MSP8a; Fig. 6e). Flanked by breccias beds up to 5 m thick (Fig. 6f, g) diminishing and becoming less well defined laterally; variably dominated by pumice or nonvesicular lava clasts, mainly clast supported but locally rich in fine tuff	Single outcrop at the summit of Mason Spur ('The Dome'; Fig. 3)
MSP7	pyroclastic cones and related lavas	basanite	Pyroclastic deposits formed of fine lapilli tuff and coeval intrusive magma; all outcrops are intensely eroded. Pillow lava present in outcrops (1) & (2) (see Comments, right). Lapilli tuffs in outcrop (1) pass up into agglutinate and oxidised scoria. Intrusions present in all outcrops, including columnar jointed necks and blocky-jointed irregular intrusive masses	Three outcrop localities: (1) ridge above Windscoop Bluff; (2) towards the top of the steep scree slope above 'The Island'; and (3) a tiny remnant at the SW limit of Anniversary Bluffs (Fig. 3)
MSP6	thick brown lavas and associated breccias	basanite	Thick brown lavas individually up to > 80 m thick and volcaniclastic deposits; interbedded with massive, polymict sandy breccia becoming finer grained and normally graded laterally; also coarse—very coarse sandstone and granule conglomerate	Unit MSP6 unconformably overlies MSP3 but the contact is unexposed (Fig. 7)

Table 1 (continued)

Stratigraphical unit**	Distinguishing characteristics	Composition***	Description	Comments
MSP5	water-cooled lava and associated sediments	basanite	Water-cooled lava 30 m thick with blocky, columnar & pseudopillow jointing; lava overlies > 6 m of rusty orange-brown sedimentary rocks, into which lava has sunk and deformed (see Figs S4-31, -32); sedimentary rocks massive to laminated, well sorted pebbly breccio-conglomerate formed of basaltic scoria but including pale grey trachytic lava fragments; also sandstone and pebbly sandstone beds	Single isolated locality at the top of 'Grassham Bluff' overlooking the head of 'Chute Glacier'
MSP4	pyroclastic cone	trachyte	Prominent trachytic pyroclastic cone draping trachyte lava of unit MSP2 and locally covered by spatter of unit MSP10; dips beneath unit MSP5; heavily eroded, > 80 m thick, formed of planar stratified ash-rich lapilli tuff (Fig. 6c); ash-coated lapilli abundant (up to c. 90%)	Single outcrop only, flanking SW side of 'The Dome'
MSP3	sandstones, breccio-conglomerates & capping white ignimbrites	mainly trachyte clasts; capping ignimbrites are trachytes	Predominantly sedimentary, well bedded; dominated by > 100 m of pale cream-coloured sandstones and interbedded coarse breccio-conglomerate (Fig. 6a; see also Supplementary Information S5 for description of a logged section); sequence capped by white fine lapilli tuffs (ignimbrites). Clasts up to 2 m across, almost entirely trachyte lava and lesser trachyte pumice; few slabs of trachytic fine lapilli tuff (from unit MSP1) 10 m in length; interbedded sandstones include a variety of tractional structures plus prominent dish and pillar structures (Fig. 6b). The capping deposit consists of white fine lapilli tuff (ignimbrite) 40 m thick. The isolated outlier to the NE is also occupies a deep erosional hollow; formed of two thick beds of gravelly breccia > 50–60 m thick comprising polymict gravel breccia with blocks of lava and slabs of trachyte breccia > 10 m across; upper bed is monomict trachyte breccia (likely block-and-ash-flow deposit)	Occupies gully or ravine at least 150 m deep (Fig. 7; see also Figs S4-23, S5-4). Also prominent isolated outlier > 100 m high above 'The Island'
MSP2	lava	trachyte	Probably two separate lavas, 3 & 40 m thick, non-vesicular and aphyric; prominent wavy foliation reflects a pilotaxitic texture	Two outcrops: above Windscoop Bluff and on top of Birthday Bluffs; both overlie unit MSP1 but contact not examined; Windscoop Bluff outcrop overlain by unit MSP7

Table 1 (continued)

Stratigraphical unit**	Distinguishing characteristics	Composition***	Description	Comments
MSP1	ignimbrites, breccias & intrusions	mainly trachyte; minor basanite & benmoreite	Massive to rare weakly stratified,strongly lithified ignimbrites, breccias and abundant hypabyssal intrusions (Fig. 5a-f; also illustrated by Martin et al. 2018, Figs. 4 and 5). Several clastic lithofacies are distinguished (described in detail in Table 2); hydrothermal alteration widespread. Dark grey hypabyssal intrusions are abundant, with ignimbrite often volumetrically minor; two types of intrusions are present: (1) irregular, with wavy fluidal or ill-defined margins; and (2) less abundant, well-defined coherent dykes with planar margins (Figs. 5d, e), which intrude all other lithofacies in MSP1. Clastic dykes common (Fig. 5f) including examples with coarse breccia fills	Dominates Mason Spur and is the oldest, thickest and most geographically widespread geological unit (Figs. 3, 4); total thickness exceeds 800 m

* See Supplementary Information S3 for full descriptions of the lithofacies

** unit numbering system, this paper

*** for major oxide compositions used to determine compositions, see Supplementary Information S2

minor in comparison and they unconformably drape MSP1 and each other. The most prominent erosional surface is at the base of unit MSP3. It defines a ravine cut at least 150 m into MSP1 (Fig. 7). Unit MSP3 is also distinctive in being largely formed of bedded sandstones and breccio-conglomerates. Sedimentary rocks are largely absent elsewhere apart from within unit MSP6 and at the base of unit MSP5, although they are just a few meters thick in the latter. Compositions at Mason Spur are essentially bimodal (basanites/tephrites to trachytes; Martin et al. 2010, 2013, 2021a, b; Supplementary Information S2). However, trachyte magmas dominate basally whilst mafic magmas were erupted mainly after unit MSP4 and form the higher part of the succession.

Chronology

Results of previous studies

Wright-Grassham (1987) determined K–Ar ages for two samples from Mason Spur equivalent to our unit MSP1 (Table 3). Another three samples from the same unit were dated by $^{40}Ar/^{39}Ar$ to try and counteract possible effects of the pervasive alteration affecting MSP1 and yielded ages consistent with the K–Ar ages. Martin et al. (2010) also published one K–Ar and two $^{40}Ar/^{39}Ar$ ages, for samples obtained within our MSP1. All of the previously determined ages for MSP1 are for the less altered intrusive units. They have a wide range of 12.80–11.4 Ma, with high 2σ errors (typically 0.2–0.4 Ma). A benmoreite sample, also dated by Martin et al. (2010) and from a location within our MSP1, yielded an age of 12.1 ± 0.2 Ma. Only two of the younger units were dated, yielding K–Ar ages of 11.7 ± 0.4 Ma for MSP7 and 6.13 ± 0.20 Ma for MSP8. Additionally, a sample of lava from Helms Bluff was dated by Wright-Grassham (1987) as 4.51 ± 0.31 Ma (by K–Ar).

Results of new $^{40}Ar/^{39}Ar$ dating

Twenty-one samples were dated by $^{40}Ar/^{39}Ar$ (Table 3; Supplementary information S1). Eight of the eleven eruptive units identified at Mason Spur are now dated, and the undated units (MSP2, MSP3, and MSP4) are stratigraphically above or below dated units so their ages are approximately constrained.

Units dated directly

Twelve samples from unit MSP1 were dated. The 2σ errors on the new ages are smaller than those already published, and range from 0.01 to 0.07 Ma (Supplementary information S1). All the new ages for MSP1 were determined on intrusions, which provide minimum limiting ages for MSP1.

Table 2 Characteristics and interpretation of clastic lithofacies in unit MSP1

Lithofacies	Characteristics	Interpretation	Comments
Massive fine lapilli tuff with flattened pumice bombs	Monomict (trachytic) fine pumice lapilli tuff; generally conspicuous flattened juvenile bombs with flattening indices (thickness divided by length) up to 0.03; generally abundant fine ash matrix, up to c. 25%; very localised faint planar bedding that fades out laterally into massive lapilli tuff; pumice lapilli typically 3 mm to 3 cm, often asociated with up to 20% perlitised obsidian lapilli 1–2 cm in diameter; ash-coated obsidian lapilli locally prominent but otherwise rare; a distinctive variant comprises abundant compressed bombs with only minor fine ash matrix in rare laterally discontinuous units 20 m thick; bombs in the latter have black glassy rims and measure 2–50 cm thick and up to 2 m long; units fade out laterally over c. 50 m into lapilli tuff with much more dispersed flattened bombs; elutriation pipes observed at one locality; Liesegang rings prominent locally at Windscoop Bluff	Deposits represent ignimbrites transported and deposited progressively mainly by granular fluid-based currents (sensu Branney and Kokelaar, 2002); massive nature may be mainly a secondary effect caused by caldera collapse; see Martin et al. (2018) for more detailed explanation	Vesicles in the flattened bombs are usually spherical signifying volatile expansion after deposition; the distinctive bomb-rich variant is probably that described by Wright-Grassham (1987), p. 39) as '*massive bomb lapillistones and agglutinate*' in her unit MS2
Massive fine lapilli tuff with flattened obsidian bombs	Distinctive variation of the fine lapilli tuff with flattened bombs lithofacies; at least 80 m thick; comprises massive monomict trachytic lapilli tuff formed of finely vesicular angular pumice lapilli 2 mm to 1 cm in diameter, varying up to 5 cm, associated with 10–20% blocky obsidian lapilli; variably clast-supported to matrix-supported with < 10–20% fine ash matrix; distinguished by the presence of 10–15% conspicuous elongate, finely fractured obsidian bombs, many with wavy fluidal shapes; other obsidians angular, partly broken or jigsaw fractured; the largest obsidian bomb seen is c. 2 m long but most are c. 20–80 cm in length	Ignimbrite deposit with obsidian spatter incorporated when pyroclastic density current overran co-erupting spatter fountain in separate vent; see Martin et al. (2018) for more detailed explanation	Only observed at the east end of Windscoop Bluff; probably the deposit described by Wright-Grassham (1987, p. 42) as '*massive, matrix-rich, obsidian-bearing lapilli tuff containing lobes of trachytic lava, with spalling obsidian rinds*' within her unit MS5 and which she interpreted as a trachytic hyaloclastite associated with local dyke intrusion into ice or water; reinterpreted by Martin et al. (2018)

Table 2 (continued)

Lithofacies	Characteristics	Interpretation	Comments
Stratified fine lapilli tuff and fine tuff	Stratified fine lapilli tuff and fine tuff lacking bombs; bedding locally very steep (up to 65°); stratification on a scale of a few mm to c. 1 decimetre, wavy planar, with low-angle dune bedforms and multiple erosional surfaces locally well developed; one bed at Windscoop Bluff shows small lapilli penetrating an underlying fine ash layer and associated small sag structures; beds commonly deformed; some are affected by syn-sedimentary faults, with fine tuff back-injected up fractures; some beds fragmented with polygonal blocks of planar laminated fine lapilli tuff up to 20–40 cm across, with rounded margins, dispersed in massive fine lapilli tuff	Deposits represent diffusely stratified and thin-bedded ignimbrites transported mainly by traction in fully dilute (low concentration) pyroclastic density currents (sense Branney and Kokelaar, 2002); broken beds are thixotropic and together with varied bed orientations indicate pervasve deformation of a stratified sequence probably linked to caldera collapse; miniature sag structures below lapilli signify ballistic deposition of lapilli falling onto a cohesive, probably moist ashy substrate	Only observed at north-west Windscoop Bluff within massive fine lapilli tuff with flattened bombs lithofacies, and at western Anniversary Bluff within massive coarse breccia; possibly corresponds to a deposit of '*thinly bedded, normally graded, airfall tuffs …. interbedded with thin, laminated and cross laminated tuff and lapilli beds with antidune structures*' described by Wright-Grassham, 1987, p. 40) in her unit MS2 and attributed by her to deposition from base surges in a tuff cone
Massive fine breccia and tuff breccia	Variably matrix- to (mainly) clast-supported monomict breccia with scarce large flattened bombs; mostly composed of lapilli-size clasts but locally composed of numerous (to 15%) angular blocks of foliated (pilotaxitic) trachyte up to 1 m in diameter; matrix is fine to coarse ash, 5–10%; lapilli are creamy white, non-vesicular and angular but some show corner abrasion; generally scarce bombs are up to 60 cm in length and have very variable concentrations up to 40%; they have deformed fluidal shapes with flattened vesicles and broken terminations	Massive monomict nature and textural and compositional similarity to associated intrusions suggests the breccias are broken & disrupted intrusions that were emplaced prior to caldera collapse; ash-matrixed variants may have undergone transport as mass flows; deposits with pumices and pumiceous bombs indicate dynamic mixing with unconsolidated ignimbrite deposits	
Massive coarse breccia	Monomict coarse breccia with angular platy clasts 2–22 cm in diameter composed of multi-coloured (pale grey, cream, rusty) weakly foliated trachyte lava; also dispersed blocks of the same up to 70% set in c. 15% to rarely 30% granule-grade matrix; locally rich in fine ash (generally c. 25; to 70%) with floating blocks; bombs absent; also occurs rarely as lenses with erosive bases within fine lapilli tuff lithofacies at Windscoop Bluff	Mainly formed by in situ disintegration of coeval pre-caldera intrusions, disaggregated during caldera collapse; often grade laterally into jigsaw-fractured and unbroken intrusions; less common ash-matrixed breccias probably transported as mass flows but no orginal bedding observed	Most widely developed at Anniversary Bluff; essentially a coarser version of massive fine breccia and tuff breccia lithofacies but lacking admixed pumiceous ignimbrites

No material from pumice within the ignimbrites was suitable given their highly altered condition. The range of ages is 12.62–11.19 Ma, similar to the age range reported by Wright-Grassham (1987) and Martin et al. (2010). The new ages suggest that most of the intrusions (c. 60%) were emplaced between 12.62 and 12.13 Ma. The intrusive period was followed by a short lull before renewed activity between 11.97 and 11.19 Ma. The intrusions in MSP1 are mainly trachytic but a few intrusions are less evolved (e.g., alkali basalt, hawaiite) and less altered. All the new ages are from samples of trachyte intrusions except for a single alkali basalt intrusion that yielded an age of 11.33 ± 0.03 Ma.

Unit MSP5 (water-cooled basanite lava), which unconformably overlies MSP1, is 12.1 ± 0.1 Ma, and 11.4 ± 0.1 Ma was obtained for a sample of lava in MSP6. Samples from two of the three outcrops of MSP7 (basanitic pyroclastic cones) were dated and yielded $^{40}Ar/^{39}Ar$ ages of 10.5 ± 0.03 and 10.02 ± 0.05 Ma. Unit MSP8 (trachyte dome) has an age of 6.03 ± 0.01 Ma.

Only a single age was obtained for outcrops of unit MSP9 (basanitic spatter and water-cooled lavas). It was determined on a sample of clastogenic lava within scoria and agglutinate and yielded an age of 0.94 ± 0.03 Ma. Unit MSP10 has yielded a single age of 0.366 ± 0.017 Ma, consistent with the relatively fresh appearance of some of the scoria cones that form MSP10, in which craters are preserved in at least two outcrops.

Finally, the middle lava-fed delta unit at Helms Bluff is 4.92 ± 0.04 Ma. Similar lithofacies at Helms Deep gave an age of 0.043 ± 0.0052 Ma.

Outcrops with bracketed ages

From the field relations and ages of dated units, units MSP2, MSP3, and MSP4 are younger than unit MSP1 and older than unit MSP5 (12.1 ± 0.1 Ma). MSP2 is older than MSP4 but otherwise the relative order of superimposition of the three undated units is uncertain. It is notable that the wide range of ages for MSP1 (12.62–11.19 Ma; all for intrusions) overlaps with that inferred for the three undated units and also units MSP5 and MSP6 (12.1 ± 0.1 and 11.4 ± 0.1 Ma, respectively), all of which unconformably overlie MSP1, a problem that is discussed later.

Interpretation of the lithofacies, and eruptive and depositional conditions of the mapped units

Unit MSP1

MSP1, the > 800 m-thick basal unit at Mason Spur, is dominated by ignimbrite and breccia deposits and numerous hypabyssal intrusions (MSP1). The ignimbrites are strongly lithified due to the pervasive clay alteration of the volcanic glass (Tables 1, 2; Supplementary Information S3). They are fines-rich, pumiceous, and are overwhelmingly massive but they include isolated relicts of diffuse stratification. In overall characteristics, they resemble the deposits of both low- and high-concentration pyroclastic density currents (Branney and Kokelaar 2002). The stratification has varied attitudes (generally steeply-dipping [> 60°]; Fig. 5b) and there are rare thixotropic textures, which suggest that the ignimbrites were more pervasively stratified originally but lost their stratification while poorly lithified, possibly through one or more deformation events (described below). Obsidian is also locally prominent, particularly in a spectacular deposit at Windscoop Bluff. That deposit has been interpreted as a spatter-rich pyroclastic density current deposit, which formed in unusual circumstances, i.e., co-eruption of ignimbrite and trachytic spatter in separate vents and mingling of the different products during transport (Martin et al. 2018).

Fine and coarse breccias are often prevalent in MSP1. They are formed of monomict, dense, fine, and aphanitic trachyte lava clasts that are texturally and compositionally identical to the massive hypabyssal intrusions (Martin et al. 2018). There is also a textural gradation from jigsaw-fractured trachyte to orthobreccia or rare parabreccia, sometimes within the same intrusion although, in general, large outcrop areas are simply formed of massive breccia. Although mingling of pumice with trachyte clasts derived from associated breccias occurs, scoriaceous trachyte lava clinkers and oxidised clinkers, characteristic of subaerial lavas, are absent. Moreover, traced up the outcrop, the individual breccia outcrops are tens of metres thick, implying that they would always have to be derived from lavas of a similar thickness, which would be unusual. Despite the brecciation, the clasts in the breccias are crystalline and do not have glassy margins, and there is no clear evidence for water chilling. The fragmentation is therefore thought to be due to deformation rather than rapid cooling. We suggest that the breccias represent progressively broken and disrupted hypabyssal intrusions that were affected by one or more volcano-tectonic (caldera-forming) deformation events, presumably the same one(s) that affected the ignimbrites. As such, they can be called collapse breccia deposits.

More clearly intrusive lithofacies are also abundant within unit MSP1. They are of two types based on morphology: (1) those with fluidal shapes; and (2) planar sheet-like intrusions. Category (1) intrusions are distinctive, with their irregular fluidal shapes signifying intrusion into an unconsolidated host. The category (1) intrusions and the massive brecciated intrusions just discussed are also extensively intruded by clastic dykes. Category (2) intrusions form tabular sheets with conspicuous fine-grained chilled margins.

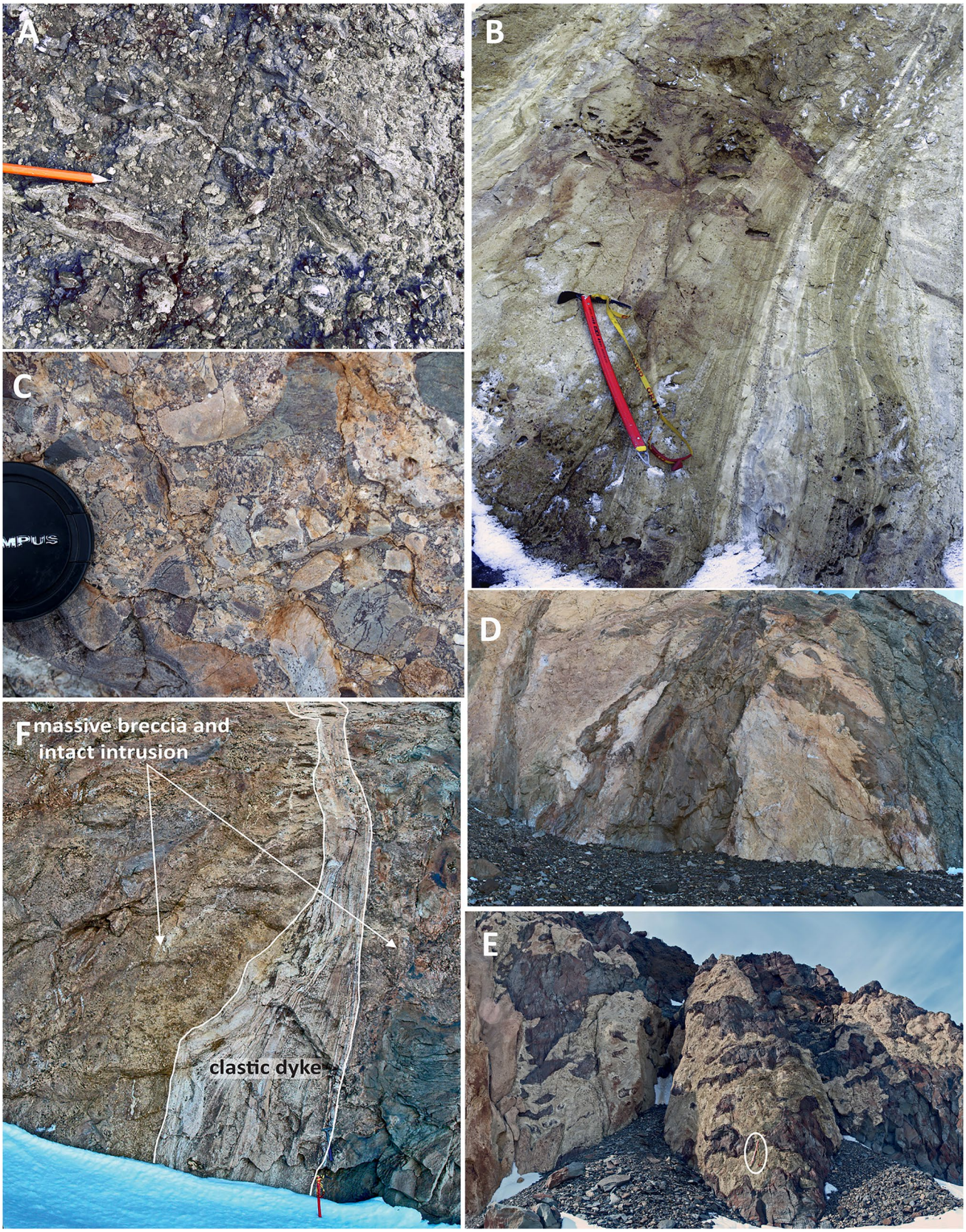
A
B
C
D
E
F
massive breccia and
intact intrusion
clastic dyke

◂**Fig. 5** Images of lithofacies within MSP1. See Tables 1 and 2, and Supplementary Information S3 for full descriptions of the lithofacies shown. (A) Close view of ignimbrite with numerous strongly flattened pumices; the length of pencil shown is c. 7 cm; Windscoop Bluff. (B) Steeply dipping thin-bedded fine- and medium-grained tuffs (ignimbrites); the sequence shows eroded surfaces and low-angle cross stratification in dune bedforms with amplitudes c. 15–20 cm and extending c. 1.5 m; the ice axe is 70 cm long; Windscoop Bluff. (C) Monomict lava orthobreccia formed of angular trachyte clasts set in c. 15% granule-grade matrix; the lens cap is 6 cm in diameter; Anniversary Bluff. (D) View of pale fawn-coloured massive breccia (brecciated intrusion) intruded by multiple dykes; fluidal dykes are cross-cut by thicker steeper sheet-like dykes; the thickest dyke in the center is c. 4 m wide; Birthday Bluffs. (E) Gray-brown fluidal trachyte lava masses intruding pale fawn-colored massive ignimbrites; the ice axe (ringed) is 70 cm long; Windscoop Bluff. (F) Prominent pale fawn-colored stratified clastic dyke cutting masses of intact intrusion and breccia; the stratification in the clastic dyke is wavy, with numerous shallow eroded cut-out surfaces; it extends at least 40 m up the cliff; an annotated closer view of this dyke is shown in Figure S4-16; ice axe for scale at lower right; Birthday Bluffs

They appear to be unaffected by tectonism and they are not intruded by clastic dykes, but their trachytic compositions indicate a compositional affinity with the earlier trachytic magmatic activity.

Units MSP2 to MSP7

Units MSP2 to MSP7 all represent short-lived small-volume eruptions. Unit MSP2 comprises at least two subaerial trachyte lavas that lack evidence for interaction with water and were erupted subaerially. They crop out at significantly different elevations and locations and hence probably represent two separate emplacement events. MSP3 is one of the most highly distinctive units at Mason Spur. It is dominated by epiclastic sedimentary rocks, comprising coarse-grained mass flow deposits and sandstones. An outlier of MSP3 also contains a massive, thick (> 60 m), polymict mass flow deposit with some clasts > 20 m in diameter and a > 50 m-thick monomict bed composed of fines-poor pumice and blocky lava clasts that is probably a block-and-ash-flow deposit related to a coeval trachyte dome that is either not exposed or no longer preserved. Most of the deposits within MSP3 have the characteristics of lahar deposits, particularly the distinctive mixture of angular and abraded clasts (hence their description as breccio-conglomerates). The mixture was probably caused by bulking up of juvenile debris (angular) with alluvial detritus (abraded) scoured from the surface over which they passed (Pierson et al. 1990; Thouret 1990; Pierson and Waitt 1999a), although shear and associated clast—clast and clast—substrate collisions in the moving flow probably also contributed to abrasion (Scott 1988). The abundance of monomict, fine, and aphanitic (juvenile?) trachyte clasts in the coarse beds also suggests a plausible link with a lava dome undergoing gravitational collapses, that transformed downslope to lahars (cf. Trabant et al. 1994; Pierson and Waitt 1999a, b). The distinctive sandy beds with faint planar lamination and spectacular dewatering structures are interpreted as products of hyperconcentrated flows also linked to lahars (i.e., lahar runout deposits; Scott 1988; Pierson and Scott 1985; Scott et al. 1995; Procter et al. 2021). Better-sorted interbeds with prominent channels and trough cross bedding represent more normal streamflow conditions recurring between lahar events and involving migrating irregular bars similar to high-gradient, gravel-dominated braided stream or river deposits (e.g., Miall 1977).

Despite the absence of any primary landform, the features of MSP4 (e.g., abundant variably vesicular blocky—angular sideromelane, fine ash matrix, lack of bedrock clasts) suggest that the deposit is hydrovolcanic in origin and is probably a relict tuff cone (e.g. Sohn 1996; Sohn et al. 2012; Brand and Brož 2015). The combination of bedding orientations and rare directional bomb sags in the ridge summit outcrops, together with a proximal spatter-rich bed and associated bedding dipping steeply (32–50°) to the southwest at the main cliff edge, implies that the vent responsible for MSP4 was probably situated somewhere beyond the cliff edge and is now eroded. MSP4 is overlain by unit MSP5, which is dominated by a thick (> 30 m) basanite lava showing prominent basal blocky and pseudopillow joints characteristic of water-cooling. The lava overlies c. 2 m of stratified pebbly sandstone and sandstone into which parts of the lava have sunk and interacted, deforming the stratification. The sediments are well sorted, nearly monomict and probably fluvial. They also contain numerous conspicuous white pumice clasts probably derived from underlying unit MSP4. Massive breccio-conglomerate > 4 m thick underlies the stratified section and may be a mass flow deposit. Unit MSP6, representing an effusive episode of substantial basanite lavas at c. 11.4 Ma, overlies MSP3 and is also associated with mass flow deposits broadly similar to the coarse lahar deposits of unit MSP3 but finer, sandier, and polymict. The two units are separated by an unconformity.

Unit MSP7 comprises deeply eroded pyroclastic cone remnants dated at 10.5 and 10.02 Ma. Reasoning similar to that used for MSP4 suggests that they were also tuff cones. Lapilli tuffs in the MSP7 outcrop above "The Island" are generally massive or show faint deformed stratification. Some of the disturbance was possibly caused by intrusion of a coeval hypabyssal neck present nearby, but the predominantly massive nature of the deposit is unusual for tuff cones, which are typically well stratified. The lapilli tuffs may thus represent a within-vent deposit homogenised by multiple explosive episodes and passage of upward-moving debris jets (White and Ross 2011; Smellie et al. 2018). However, a thin sequence of stratified tephra beds with bomb and impact sags is prominent in mid-elevation

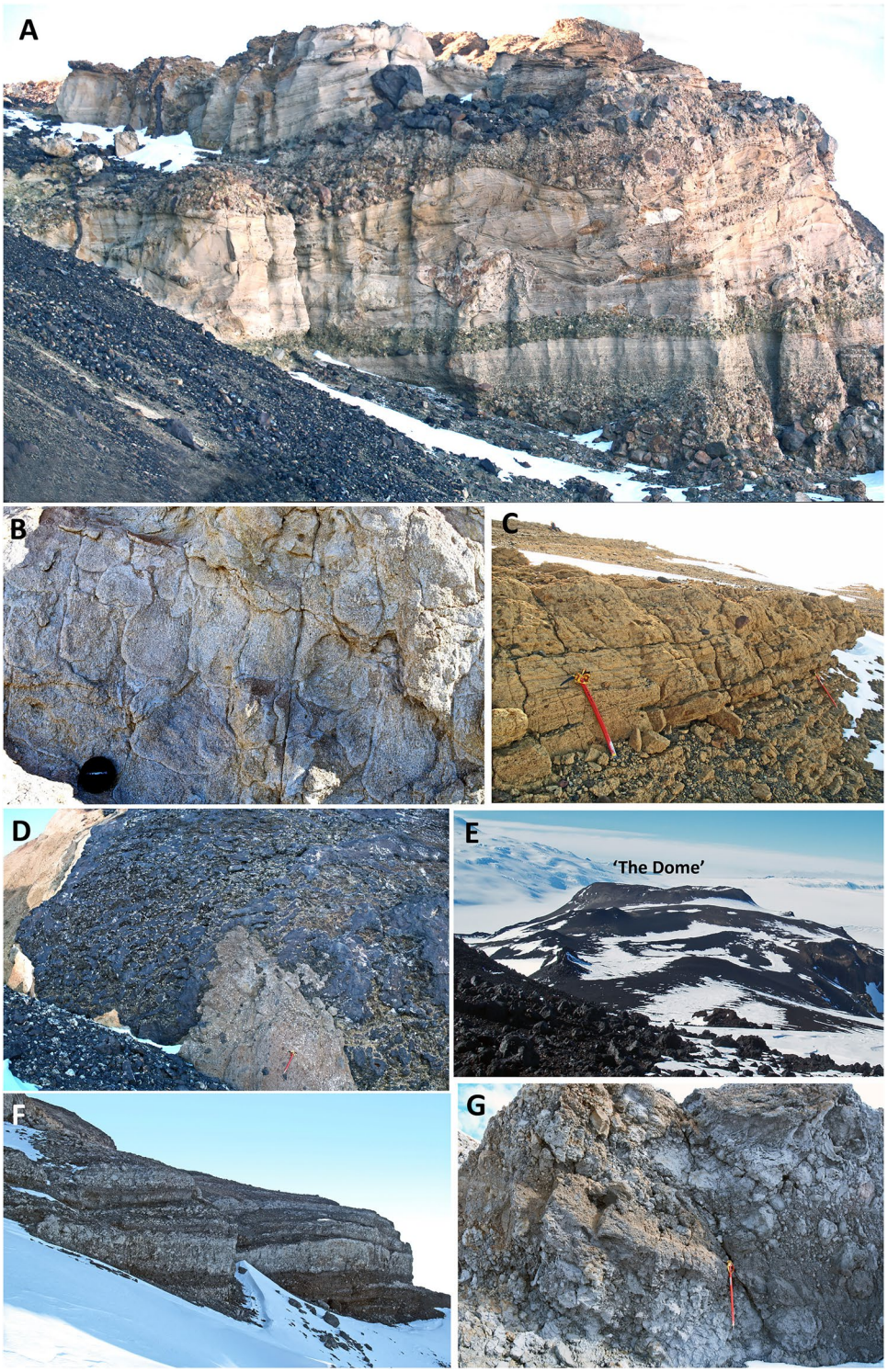

Fig. 6 Images showing features of units MSP3 to MSP8. See Table 1 and Supplementary Information S3 for full descriptions of the units shown. (A) Cliff face c. 60 m high cut in MSP3 showing alternating coarse boulder and cobble breccio-conglomerates and off white-colored sandstones with numerous trough cross stratified channels; Anniversary Bluff. (B) Very coarse sandstone showing prominent water-escape (dish-and-pillar) structures; MSP3; the lens cap is 6 cm in diameter; Anniversary Buff. (C) Diffusely planar-stratified trachytic lapilli tuffs (MSP4); the deposits contain abundant ash-coated lapilli; the ice axe is 70 cm long; above Birthday Bluffs. (D) Dark gray basanite pillow lava intruding pale yellow-coloured basanitic lapilli tuffs; the contacts show abundant evidence of soft-sediment deformation caused by intrusion of the pillow lava; MSP7; above "The Island." (E) View looking east north-east to "The Dome," a prominent flat-topped, steep-sided trachyte lava dome 900 m in diameter (MSP8). (F) 25 m-high cliff face cut across thick-bedded coarse trachyte breccias (block-and-ash-flow deposits) of MSP8; the prominent topographical shoulder at upper left is the margin of the coeval lava dome; the conspicuous thick pale bed near the centre of the cliff face is c. 5 m thick. (G) Close view of pumiceous block-and-ash-flow deposits seen in (F)

exposures. The stratification is steep-dipping (28°) and the unit may represent a large coherent stratified slab, measuring c. 12 m thick and 40 m in length, that slid into the vent (cf. White and Ross 2011).

Units MSP8, MSP9, and MSP10

Unit MSP8 is a small trachyte lava dome. It is associated with thick beds alternately dominated by pumice or

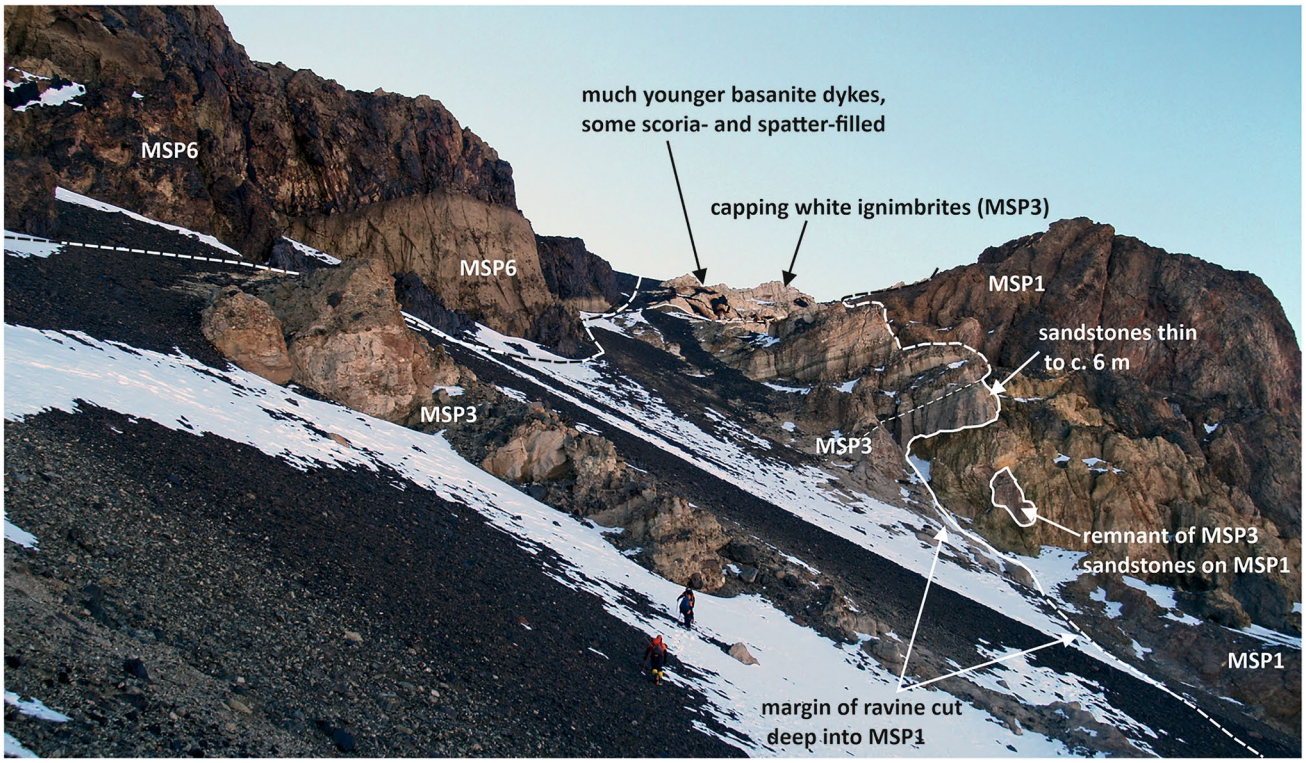

Fig. 7 View of stratified unit MSP3 and its stratigraphical relationship with unit MSP1, looking east from the west end of Anniversary Bluff. MSP3 deposits fill a deep ravine cut in MSP1 and are overlain by basanite lavas and pale khaki-colored mass flow deposits of MSP6. The contact between MSP3 and MSP6 is erosional. White trachytic ignimbrites that cap unit MSP3 in the background are missing in the foreground. Note the prominent dip to the left (north-west) of stratification within unit MSP3 indicating that deformation has occurred. The true dip is less than that shown and is over-emphasized due to camera foreshortening (cf. Fig. 6a)

fine-grained crystalline lava blocks interpreted as explosively-generated block-and-ash-flow deposits derived by collapses of "The dome." The oxidized surfaces shown by some of the pyroclastic beds and the surfaces of bombs and some breccia masses in the block-and-ash-flow deposits are consistent with emplacement at high temperatures.

The eruption of unit MSP9 began with effusion of basanitic lavas with distinctive joint patterns indicative of water cooling. However, other products of MSP9 and all of MSP10 consist of scoria cones and associated agglutinate and clastogenic lavas. MSP9 is dated as 0.94 Ma. Although Wright-Grassham (1987) obtained a K–Ar age of 11.7 ± 0.4 Ma apparently within the MSP9 outcrop to the south-east of The Dome (MSP8), our mapping suggests that it probably dates a small isolated outlier of MSP7 basanitic spatter, several of which crop out on this slope above the main MSP7 outcrop (Fig. 4). The locations of the vents responsible for unit MSP9 are unknown. Some were probably situated on the Mason Spur ridge crest, although others may have been fed by the scoria and spatter-filled dykes which cut MSP1 (see Fig. 7 and S4-20–22). It is also conceivable that some vents are represented by scoria cones assigned to MSP10. However, most of the MSP9 outcrops are > 1 km from known MSP10 vents, which is probably too far for accumulation of spatter and agglutinate erupted from those centres. Scoria cones in MSP10 have an east-northeast—west-southwest alignment and were probably erupted from fissures.

Un-numbered units

Additional basanite outcrops, mainly massive breccias, occur at Helms Bluff, Snow Petrel Peak (4.9 Ma) and Helms Deep (0.04 Ma). The thickness and lithology of the breccia deposits, together with their abundant irregular lava masses with blocky jointing characteristic of water cooling, strongly resemble the chaotic lava-lobe-bearing breccia lithofacies that characterises the basal subaqueously-deposited lithosome of glaciovolcanic 'a'ā lava-fed deltas (Fig. 8e, f; Smellie et al. 2011a, b, 2013; Smellie and Edwards 2016). The breccias at Helms Deep lack any capping lavas (presumably eroded) but pāhoehoe lavas capping poorly exposed breccia(?) deposits are seen in the cliff close to the Helms Deep outcrop and probably represent an underlying pāhoehoe lava-fed delta. The outcrops at Snow Petrel Peak and Helms Bluff pass up into capping 'a'ā lavas and are 'a'ā lava-fed deltas.

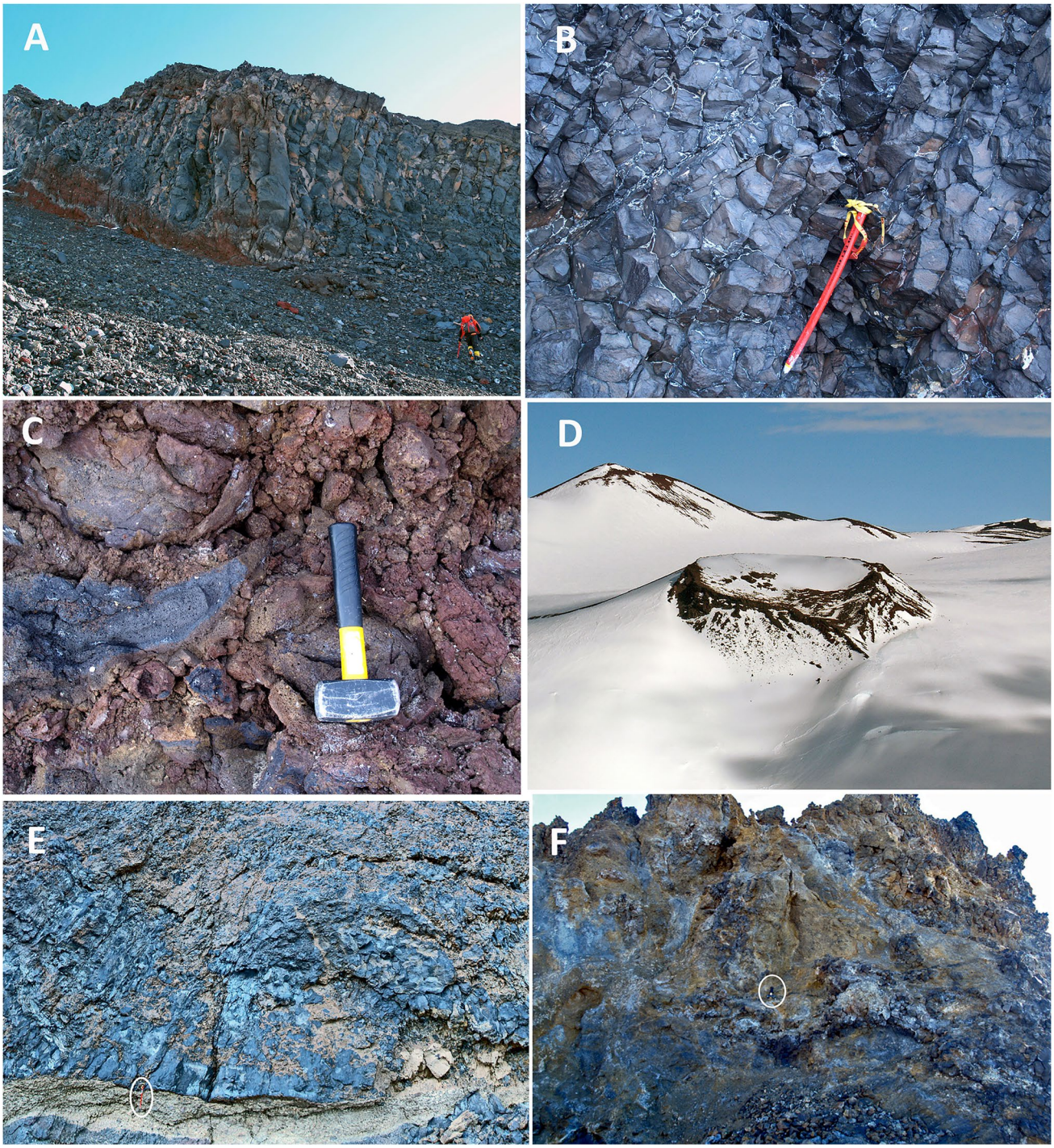

Fig. 8 Images showing features of units MSP9, MSP10 and lava-fed deltas. See Table 1 and Supplementary Information S3 for full descriptions of the units shown. (A) View of thick basanite lava (MSP9a) draping a steep slope above Anniversary Bluff; the lava shows crude thick prismatic cooling columns up to 2.5 m in diameter and overlies strongly reddened agglutinate; the lava crag is c. 20 m high. (B) Blocky-jointed (water-cooled) basanite lava (MSP9b) draping the steep slope north-west of Windscoop Bluff; the ice axe is 70 cm in length. (C) Flattened and globular coarsely vesicular bombs in agglutinate forming a large scoria cone c. 2 km north-west of "The Dome" (MSP10); the hammer is 25 cm in length. (D) Scoria cone with a well-preserved crater c. 300 m across, and steep eroded outer flanks (MSP10); the hills in the background are more-degraded examples of scoria cones assigned to MSP10. (E) Chaotic basanitic pillow lava masses and aphanitic breccia at the base of the middle sequence at Helms Bluff; the deposit resembles the subaqueous lithosome of an 'a'ā lava-fed delta; the orange-coloured deposit is a lapilli tuff probably reworked from some very large rock masses carried by the delta as it advanced (cf. Smellie and Rocchi 2021, figs. 8, 12); ice axe (ringed) gives scale. (F) Chaotic blue-grey and dark grey basanite lava masses and rust-coloured aphanitic breccia, interpreted as the subaqueous lithosome of an 'a'ā lava-fed delta; the hammer near centre of the photograph (ringed) is 25 cm in length; Helms Deep (Dunbar Head)

Table 3 Published and new isotopic ages for volcanic units at Mason Spur

Sample	Unit**	Dated lithology	Age (Ma)	±2σ (Ma)	method	laboratory***	Comments
THIS PAPER							
AM17024	MSP10	Lava, basanite	**0.366**	**0.017**	Ar–Ar, groundmass	IGG	clastogenic
AM17047	MSP9	Lava, basanite	**0.939**	**0.027**	Ar–Ar, groundmass	IGG	drapes steep slope
AM17026	MSP8	Lava dome, trachyte	**6.028**	**0.008**	Ar–Ar, groundmass	IGG	
AM17039	MSP7	Pillow lava, basanite	**10.017**	**0.045**	Ar–Ar, groundmass	IGG	intrudes coeval lapilli tuffs
AM17032	MSP7	Intrusion, basanite	**10.503**	**0.034**	Ar–Ar, groundmass	IGG	intrudes coeval scoria and agglutinate in neck
AM17043	MSP6	Lava, basanite	**11.4**	**0.1**	Ar–Ar, groundmass	IGG	poor Ar spectrum
AM17046	MSP5	Water-cooled lava, basanite	**12.1**	**0.1**	Ar–Ar, groundmass	IGG	may have been fed by a category (2) intrusion within MSP1
AW83422	MSP1	Intrusion, perakaline trachyte	**11.19**	**0.04**	Ar–Ar, sanidine	NMGRL	
AM17010	MSP1	Intrusion, alkali basalt	**11.329**	**0.026**	Ar–Ar, groundmass	IGG	
AW85847	MSP1	Intrusion, perakaline trachyte	**11.46**	**0.05**	Ar–Ar, sanidine	NMGRL	
AM17018	MSP1	Intrusion, trachyte	**11.695**	**0.037**	Ar–Ar, groundmass	IGG	
AW83678	MSP1	Intrusion, perakaline trachyte	**11.97**	**0.05**	Ar–Ar, sanidine	NMGRL	
AW83503	MSP1	Intrusion, perakaline trachyte	**12.13**	**0.06**	Ar–Ar, sanidine	NMGRL	
AW83508	MSP1	Intrusion, perakaline trachyte	**12.16**	**0.03**	Ar–Ar, sanidine	NMGRL	
AW83701	MSP1	Intrusion, trachyte	**12.19**	**0.07**	Ar–Ar, sanidine	NMGRL	
AW83511	MSP1	Intrusion, perakaline trachyte	**12.29**	**0.04**	Ar–Ar, sanidine	NMGRL	
AM17002	MSP1	Intrusion, trachyte	**12.312**	**0.029**	Ar–Ar, groundmass	IGG	poor Ar spectrum; preferred weighted mean age **12.29 Ma**
AM17014	MSP1	Intrusion, trachyte	**12.392**	**0.033**	Ar–Ar, groundmass	IGG	
AM17034	MSP1	Intrusion, trachyte	**12.616**	**0.013**	Ar–Ar, groundmass	IGG	likely category 1 intrusion (see text for explanation), with fluidal margins
AM17023	['Helms Deep']	Lava, basanite	**0.043**	**0.0052**	Ar–Ar, groundmass	IGG	water-cooled lava mass within aa lava-fed delta; delta sourced from Mt Morning?

Table 3 (continued)

Sample	Unit**	Dated lithology	Age (Ma)	±2σ (Ma)	method	laboratory***	Comments
AM17030	[Helms Bluff]	Lava, basanite	**4.916**	**0.044**	Ar–Ar, groundmass	IGG	subaerial capping lava of middle aa lava-fed delta; delta probably sourced from Mt Discovery
Martin et al., 2010							
OU78628	MSP1	Intrusion, trachyte	**11.4**	**0.2**	Ar–Ar	NMGRL	
OU78635	MSP1	Intrusion, comenditic trachyte	**12.6**	**0.4**	K–Ar	NMGRL	
OU78634	MSP1	Intrusion, tephrite	**12.9**	**0.2**	Ar–Ar	NMGRL	
Wright-Grassham, 1987							
AW83647	MSP8	Trachyte	*6.13*	*0.20*	K–Ar	NMGRL	
AW85839	MSP7	Benmoreite	*11.7*	*0.4*	K–Ar	NMGRL	sample probably from outlier of MSP7 within MSP9 outcrop; accuracy of age uncertain (too old?)
AW83653	uncertain, probably MSP1	Likely intrusion, peralkaline trachyte	**11.4**	**0.2**	K–Ar	NMGRL	minor but significant groundmass alteration
AW83678	MSP1	Intrusion, perakaline trachyte	**11.46**	**0.09**	Ar–Ar	NMGRL	plateau age
AW83513	MSP1	Likely intrusion, benmoreite	**12.1**	**0.2**	K–Ar	NMGRL	may have fed extrusive activity (MSP5)?
AW83712	MSP1	Intrusion, perakaline trachyte	**12.52**	**0.57**	Ar–Ar	NMGRL	plateau age (forced)
AW83569	MSP1	Intrusion, perakaline trachyte	**12.80**	**0.44**	Ar–Ar	NMGRL	plateau age
AW83614	[Helms Bluff]	Basanite	*4.51*	*0.31*	K–Ar	NMGRL	middle lava-fed delta; delta probably sourced from Mt Discovery

ages as published or as determined in this study are quoted in full in this table, but the new ages are rounded off to 2 decimal places when quoted in the text, to ensure easier comparability with the published ages. Preferred ages shown in **bold**

* see Supplemental Information S1 for analytical details of the newly-dated samples

** unit designations from this paper

*** IGG—Istituto di Geoscienze e Georisorse, Consiglio Nazionale delle Ricerche, Pisa, Italy; NMGRL—New Mexico Geochronology Research Laboratory, Socorro, USA

Discussion

This study combines the first modern in-depth assessment of the volcanic history of Mason Spur together with an improved chronology. The study is facilitated by the deep erosion of the outcrop, which has exposed a 1000-m-thick section of a volcanic complex. The current assessment is based on interpretations of the lithofacies and numerous new isotopic ages. It is currently the most detailed description of an ancient volcanic complex within the WARS. The sequence at Mason Spur is constructed from multiple volcanic and volcaniclastic eruptive units together with epiclastic sequences, which we have designated MSP1-MSP10. The activity is summarized as follows: the volcanism was mainly trachytic during Miocene time (between c. 13 and 12 Ma), represented by units MSP1 (the most voluminous unit exposed at Mason Spur), MSP2, MSP3 and MSP4. A younger phase of trachyte activity briefly recurred after a gap of c. 5 Myr with effusion of a small lava dome (MSP8). Units with basanite compositions and low volumes were erupted mainly between c. 12 and 10 Ma (units MSP1 (in part), MSP5, MSP6 and MSP7) and again in the Pleistocene epoch (after 1 Ma), following a long period of non-eruption or erosion lasting c. 9 Myr (units MSP9, MSP10). Eruptions at Mason Spur ended by about 0.37 Ma. Additional episodes of basanitic activity at c. 4.9 and 0.04 Ma are represented in flanking outcrops at Helms Bluff, Snow Petrel Peak and Helms Deep. However, they were probably sourced from vents on the Mount Morning and Mount Discovery volcanoes, which have comparable eruption ages (Martin et al. 2010; Smellie and Martin, 2021). At least four major eruptive stages are recognized and are described below (Fig. 9).

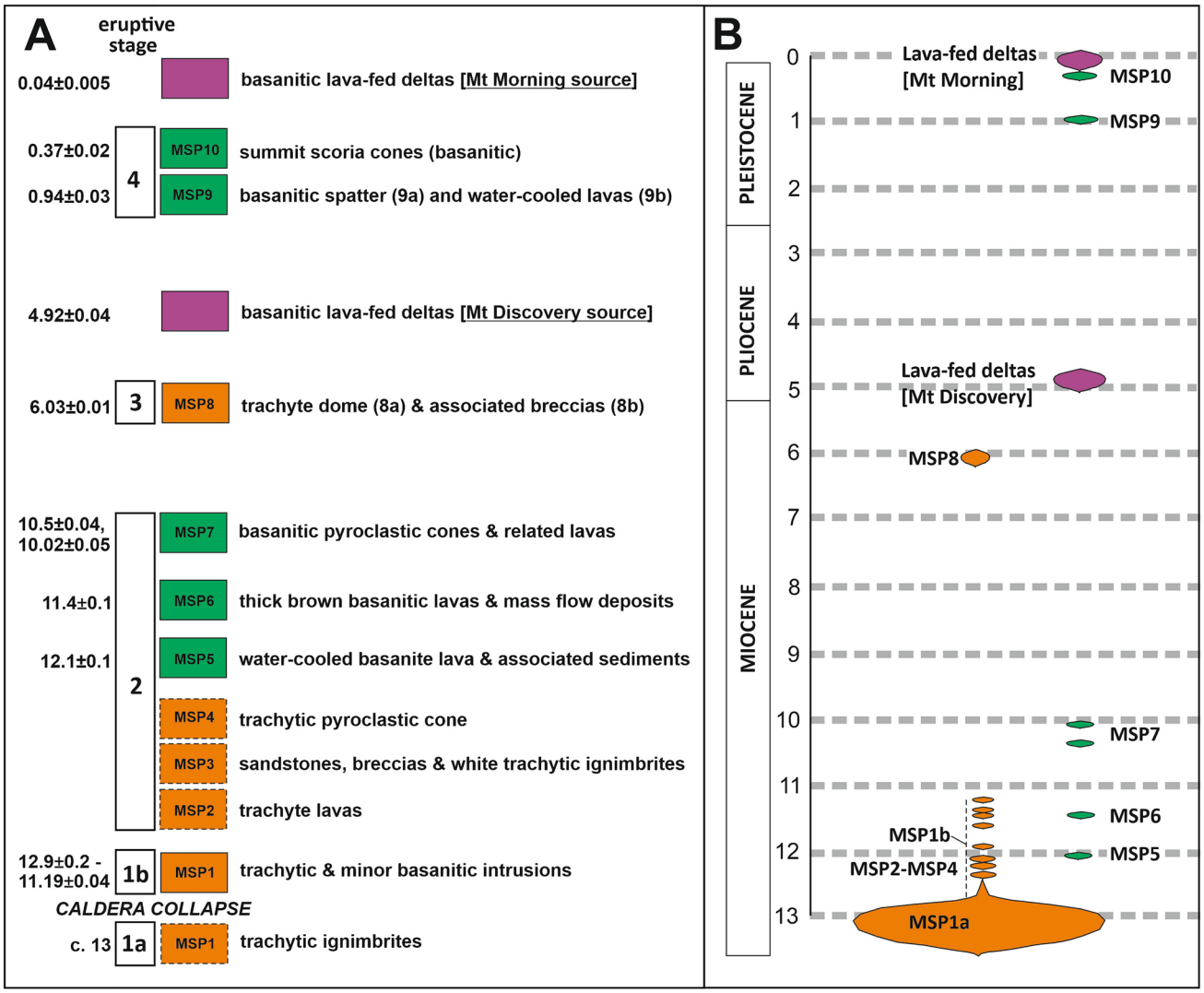

Fig. 9 (A) Diagram showing the stratigraphical succession exposed at Mason Spur based on this study. The descriptive eruptive stages used in this paper are also shown (see text and Table 1 for details). The ages of MSP1 ignimbrite eruptions, MSP2, MSP3, and MSP4 are known only indirectly (bracketed by other dated units) and are indicated by dashed-line boxes. Orange coloration represents trachytic units; green represents basanitic or alkali basalt units; purple represents basanitic units extrinsic to Mason Spur. (B) Schematic diagram illustrating the different erupted volumes associated with each of the stratigraphical units. Not to scale but the sizes of the colored objects are intended to crudely represent the different magma volumes associated with each eruptive episode. The most voluminous volcanic episode is represented by trachyte unit MSP1, with a volume exceeding 85 km^3. All other units represent short-lived small-volume eruptions of trachyte or basanite magmas apart from relatively voluminous effusive events represented by lava-fed deltas flowing from centres on Mount Discovery and Mount Morning

Evolution of the Mason Spur volcanic complex

Stage 1a: major trachyte volcano; pre-caldera ignimbrites and brecciated intrusions (MSP1a; c. 13 Ma)

This stage is represented by massive ignimbrites and lithic breccias. They are the oldest deposits exposed at Mason Spur and they represent the most voluminous eruptive episode of the volcanic complex. The abundant hypabyssal intrusions (see next section) and pervasive hydrothermal alteration in the ignimbrites and breccias might suggest that MSP1 is a subvolcanic (hypabyssal) complex. However, the association of abundant clastic dykes, deformation of (unconsolidated) ignimbrites and widespread massive brecciated intrusions, together with the large volume implied by the extensive thick outcrop and its pervasive alteration, indicate that unit MSP1 is probably a caldera fill (assumed by Martin et al. 2018). The deformation resulted from one or more caldera collapse events, and is also evidenced by the variable, often very steep dips (> 60°) of relict stratified

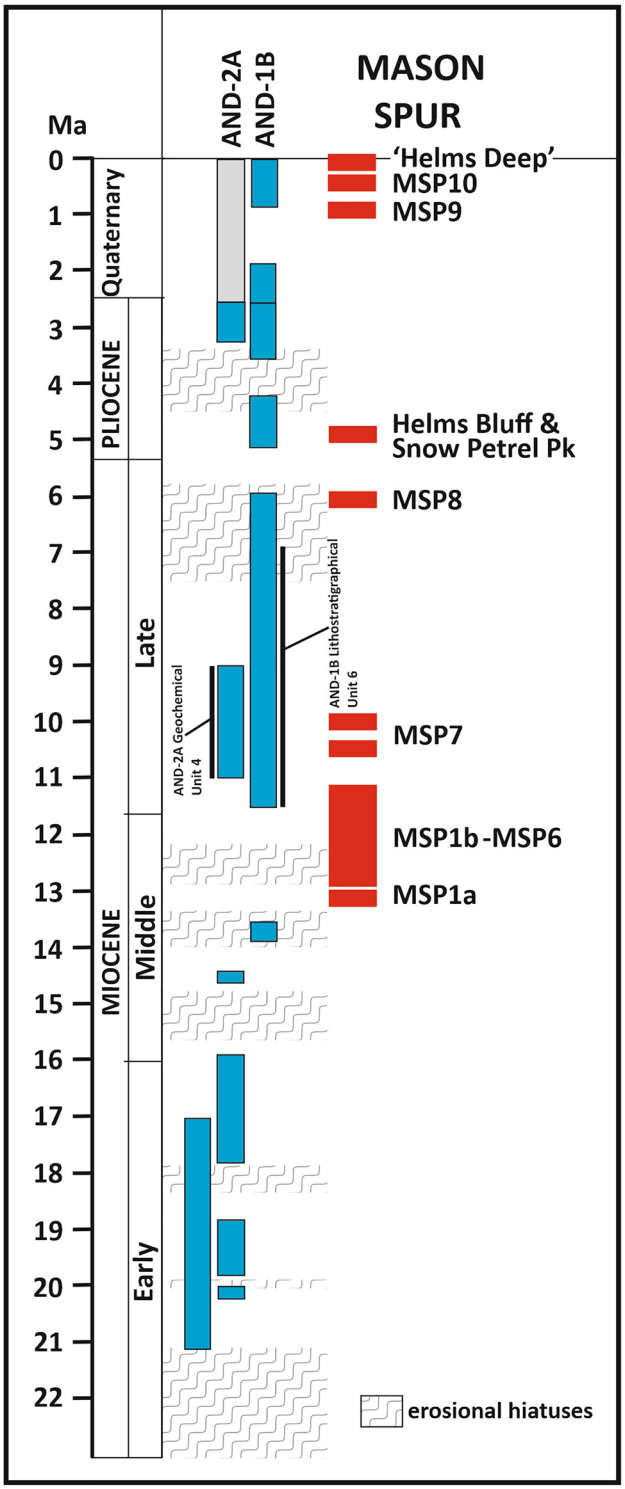

Fig. 10 Chronostratigraphical framework for strata recovered by AND-1B and AND-2A drill cores (blue bars represent relatively well dated strata; the gray bars indicate intervals for which ages are not well constrained; after Levy et al. 2021) compared with the age of volcanic episodes at Mason Spur identified in this paper (red bars). MSP1a—ignimbrites; MSP1b—intrusions. The positions of sedimentary deposits rich in volcanic detritus possibly derived from eruptions at Mason Spur (i.e., AND-2A Geochemical Unit 4 and AND-1B Lithostratigraphical Unit 6) are also shown; see text for details). The erosional hiatuses indicated represent regional seismic unconformities encountered in Ross Sea drill cores, interpreted as periods of multiple ice advances and retreats (Levy et al. 2021)

ignimbrites present. The clastic dykes, some with unusually coarse (breccia) infills, probably signify pervasive hydraulic fracturing, fluidization, and over-pressured injection during caldera settling (cf. Phillips 1972; Branquet et al. 1999). The caldera dimensions are not well defined. However, the lateral south-west—north-east outcrop extent is c. 13.5 km. With a measured minimum thickness for the deposit (ignimbrites and intrusions) of 800 m, an assumed elliptical outline and a cylindrical shape, a minimum volume of 85 km^3 is calculated for the caldera fill. The largest-known caldera elsewhere in the WARS is c. 10 km in diameter (Chang Peak volcano (rhyolite), Marie Byrd Land; Wilch et al. 2021). The Mason Spur caldera might therefore be one of the largest in Antarctica, matched only by the Holocene (c. 4 ka) caldera on Deception Island (Antarctic Peninsula; diameter 9–11 km, erupted volume c. 30–90 km^3; Martí et al. 2013; Antoniades et al. 2018; Smellie 2021).

The apparent absence of extra-caldera ignimbrites near Mason Spur may be due to the location of the volcanic centre as an island within the Ross Sea Embayment. If deposition of the extra-caldera products took place on a Miocene Ross Ice Shelf and outlet glaciers of the Transantarctic Mountains, the deposits would have been transported by ice to the ocean and effectively lost to the geological record. Alternatively, in an ice-poor or ice-free period when an ice shelf was absent, the tephras would have been deposited mainly within the Ross Sea.

The only potential source of information on coeval marine sedimentation in the area is from drill cores, AND-2A and AND-1B, obtained at sites c. 90 km north-east of Mason Spur (Fig. 1). MSP1 was probably erupted during a period represented by an erosional hiatus in AND-2A (Fig. 10). However, the hiatus was succeeded by the deposition of Geochemical Unit 4 (123–225 m below sea floor (mbsf); Panter et al. 2008; Di Vincenzo et al. 2010). Geochemical Unit 4 is largely composed of diamictite (c. 80% by volume, estimated) with subordinate conglomerate, sandstone, and siltstone. Linked petrographical and geochemical studies of the unit indicated that the clasts are dominated by volcanic rocks, and continuous XRF scanning of the core shows a simultaneous marked increase in Si; the proportion of fresh volcanic glass also shows a marked increase in Geochemical Unit 4 (Panter et al. 2008; see also Nyland et al. 2013). The clasts consist of a mixture of mafic, intermediate, and felsic compositions, including black scoria and brown (probably mafic) glass, light gray to golden brown pumice (including long-tube pumice) and intermediate and felsic clasts with pilotaxitic textures; one of the few clasts

analyzed was shown to have a peralkaline trachyte composition. The abundance of volcanic clasts increases markedly above 225 mbsf, with a prominent peak between 182 and 174 mbsf, and continues up to 30 mbsf. The available information suggests that the volcanic material in AND-2A, particularly its sudden influx, may have been strongly influenced by trachytic and subordinate mafic eruptions at Mason Spur associated with MSP1, including caldera collapse. Either the exposed edifice contributed eroded material for a long time or much of the debris was reworked up-section into younger sediments during successive glacial advances that were probably responsible for the depositional hiatus. Eruption of MSP1 ignimbrites also probably corresponds to an erosional unconformity in AND-1B (Wilson et al. 2012; Fig. 10). The closest succeeding units are two sedimentary sequences designated LSU5 and LSU6 (McKay et al. 2009); LSU5 is significantly younger than LSU6 (c. 6.5 Ma; Wilson et al. 2012) and is not relevant to MSP1. The basal part of LSU6 (c. 1250–1067 mbsf) is dominated by diamictites (> 90% by volume, estimated) with minor sandstone, whereas the upper part (c. 1067–762 mbsf) comprises mainly mudstones and sandstones with lesser diamictites (c. 25% by volume). Volcanic debris is present throughout LSU6 although it is not unusually abundant (Pompilio et al. 2007). It comprises mafic, intermediate, and felsic compositions but intermediate—felsic compositions with trachytic textures are dominant. Glass is also present and its abundance increases markedly above c. 850 mbsf. It is mainly mafic but ranges to trachyte in composition. The lower volume of volcanic detritus and the abundance of *mafic* glass in AND-1B (LSU6) compared with AND-2A may be due to different sediment transport paths to the two sites, which are 50 km apart, or else different provenances. Since most of other large volcanic centres in the area (Mount Discovery, Brown Peninsula, White Island, Ross Island; Smellie and Martin 2021) are younger than c. 5 Ma and would not have been present, the palaeotopography was undoubtedly very different at the time. Overall, a link with eruptions at Mason Spur is less obvious in AND-1B than for AND-2A but is still permissible.

Stage 1b: post-caldera intrusive activity (MSP1b; c. 12.9–11.2 Ma)

The abundant hypabyssal intrusions within unit MSP1 can be assigned to at least two intrusive episodes: (1) early post-collapse of the caldera; and (2) late post-collapse. By contrast, the massive breccias described for stage 1a are linked to the caldera collapse event, i.e., created by pervasive brecciation of pre-collapse intrusions. They are thus pre-caldera in age. The category (1) intrusions with fluidal margins intrude the ignimbrites and brecciated intrusions indicating that their emplacement post-dated the collapse, although a few show minor faults affecting their margins. Only one of our dated samples is from a category (1) intrusion. It has the oldest age in our new dataset (12.62 ± 0.01 Ma) and is almost within error of the oldest previously published age (12.9 ± 0.2 Ma; Table 3). The other dated samples were obtained on category (2) intrusions (tabular sheets with planar margins), which intrude ignimbrites, breccias and fluidal-margined intrusions. The lack of brecciation of category (1) and (2) intrusions signifies a post-collapse age. Thus, the age of the collapse event is bracketed by the age of the brecciated intrusions (pre-collapse; age unknown) and the fluidal intrusions (early post-collapse; c. 12.9 Ma). Here we take c. 13 Ma as the likeliest time for the caldera-forming event. However, the ages of category (2) intrusions extend up to 11.2 Ma (Table 3). This implies a lifetime for the basal trachyte volcano of at least 1.5 Myr and the possibility of associated trachytic ignimbrite eruptions, or small trachytic centres now removed by erosion. A lifetime of > 1.5 Myr is not unusual for a large polygenetic stratovolcano (Panter et al. 1994) but other explanations are possible (see later).

Stage 2: uplift and eruption of multiple small-volume trachyte and basanite monogenetic centers (MSP2-MSP7; c. 12.9–10 Ma)

Unit MSP1 underwent significant erosion prior to the eruption of the other stratigraphical units. It may imply a change in the local base level due to uplift of the volcano. There is no definitive evidence for uplift in the Mason Spur sequence but we note that unit MSP3, at least, has been back-tilted slightly (Fig. 7), which suggests that some deformation has occurred. Moreover, neptunian dykes filled by white ignimbrite have infilled fractures in the top few metres of the sedimentary rocks of unit MSP3 (Fig. S4-23), also consistent with deformation associated with vertical displacement(s). Mason Spur is situated on the eastern flank of the Transantarctic Mountains (Fig. 1). Different parts of the Transantarctic Mountains appear to have acted independently to phases of uplift, although there is little direct information for the period after c. 30 Ma (Fitzgerald 2002; Olivetti et al. 2018). Miller et al. (2010) suggested that uplift of c. 300–800 m may have affected parts of the Transantarctic Mountains since c. 14 Ma, based on thermochronology and geomorphology. Moreover, post-Middle Miocene Climate Transition (i.e., after 14.8–13.8 Ma) isostatic uplift of a few hundred metres might also have occurred in response to valley erosion by glaciers (Halberstadt et al. 2021; Sauli et al. 2021). Mason Spur is also situated on the margins of the so-called Discovery accommodation zone, a prominent tectonic feature that crosses the Transantarctic Mountains and separates two discrete structural blocks (Wilson 1999).

The zone acts as a natural focus for major trunk glaciers crossing the mountains and is likely to have experienced episodes of vertical movement, although poorly quantified (Wilson 1999; Olivetti et al. 2018). Mason Spur also lies within a southern extension of the Terror Rift, one of the youngest parts of the WARS (Fig. 1). The Terror Rift formed either during the Middle Miocene epoch after 13 Ma (Fielding et al. 2006; Fielding 2018) or else as a result of a change in relative plate motion forces, from orthogonal to dextral strike-slip, after 26 Ma (Granot and Dyment 2018). Faulting and associated changes in elevation are also known to have continued sporadically in the Terror Rift during Pliocene, Pleistocene, and Recent times (Fielding et al. 2006; Paulsen and Wilson 2009; Martin and Cooper 2010; Sauli et al. 2021), so changes in base level are likely to have affected Mason Spur on more than one occasion.

The erosion recorded at Mason Spur probably commenced soon after caldera collapse and recurred frequently thereafter (e.g., prior to eruption of each of the unconformably overlying units MSP2-MSP4, formed between 13 and 12 Ma), resulting in a cumulative erosional relief of hundreds of metres. The presence of intrusions with even younger ages (to 11.2 Ma) that were exhumed prior to eruption of units MSP5 and MSP6 suggests that significant erosion also occurred after 12 Ma. It seems likely that many of the category (2) intrusions (both trachytic and rarer basanites) may be feeder dykes for some of the younger units present as well as other units that have been completely eroded; the intrusions are included within MSP1 simply as a convenience because they occur within the MSP1 outcrop and are truncated by erosion.

Following eruption and caldera collapse of the large trachyte ignimbrite volcano (MSP1), trachyte and minor basanite magmas fed activity at several small centres resulting in effusion of trachyte (MSP2) and basanite (MSP5) lava flows and white trachytic ignimbrite deposits (top of MSP3), then further basanite lava flows (MSP6) and trachytic and basanitic pyroclastic cones (MSP4, MSP7). Unit MSP2 comprises subaerial trachyte lavas, which were probably erupted during two discrete effusive episodes, both undated but older than units MSP4 and MSP7 (Fig. 4). The thick sedimentary deposits of unit MSP3 infilled a deep ravine cut in unit MSP1 (Figs. 4, 7). Fluvial conditions have been inferred for some of the sediments within unit MSP3, associated with lahar and lahar runout deposits. The interbedded fluvial deposits are subordinate to other sediment types (see Supplementary Information S5). It is generally assumed that the Antarctic climate became steadily more frigid after c. 14 Ma, and rapidly transitioned to a predominantly polar glacial regime (Lewis et al. 2007). However, modelling of the Middle Miocene epoch suggests that episodes of amelioration probably also occurred, consistent with tundra conditions (Halberstadt et al. 2021), when flowing water (rivers, streams) may have developed during summers. Unit MSP6 unconformably overlies unit MSP3 and, as well as basanite lavas, it contains mass flow deposits that probably accumulated within the same ravine as MSP3. The ravine may have been rejuvenated perhaps by further uplift and downcutting. Additional magmas were erupted explosively from at least four small tuff cone centres (MSP4 [trachyte], MSP7 [basanite]), mainly after a depositional or erosional gap lasting c. 1 Myr. Finally, basanite lava flows interacted with surface water (or meltwater) at a high elevation (c. 1000 m) at 12.1 Ma (MSP5). The location of its source vent is unknown but is probably obscured by the outcrop of unit MSP8.

Stage 3: final trachyte activity (dome and block-and-ash-flow units) (MSP8; c. 6 Ma)

Effusion of a small but prominent trachyte dome (MSP8a) and associated block-and-ash-flow deposits (MSP8b) at the summit of Mason Spur marked the final pulse of trachyte volcanism at Mason Spur (Fig. 9). The event was subaerial, lacking any obvious interaction with water, and is dated at 6.03 ± 0.01 Ma, within error of the K–Ar age of 6.13 ± 0.20 Ma obtained by Wright-Grassham (1987) (Table 3).

Stage 4: multiple basanite scoria cones (MSP9, MSP10; c. 0.94 to 0.37 Ma)

Following a hiatus in volcanism potentially indicating a repose period of c. 5 Myr, younger activity at Mason Spur was exclusively basanitic and lasted sporadically until late Middle Pleistocene time. Because of its markedly younger age, the younger basanitic activity represented by units MSP9 and MSP10 probably corresponds to a fresh influx of magma. It may be related to a Pleistocene extensional tectonic phase in the Terror Rift that permitted mafic magmas to rise along deep crustal fractures (e.g., Fielding et al. 2006; Rilling et al. 2009; Sauli et al. 2021), similar to basanite magma that was sporadically erupted, in small volumes, during the Miocene stage 2 eruptive phase (Fig. 9).

Basanite lava-fed deltas sourced from neighbouring volcanoes

It has been suggested that the sequence of ‘a‘ā lava-fed deltas at Helms Bluff was probably sourced from a vent in the vicinity of Mount Discovery (Smellie and Martin 2021). Our new age for the middle sequence at Helms Bluff (4.92 ± 0.04 Ma) improves on the K–Ar age (4.51 ± 0.31 Ma) by Wright-Grassham (1987; Table 3). The Helms Bluff and Snow Petrel Peak sequences are remarkably similar,

with subhorizontal capping lavas and associated breccias each > 200 m thick. We suggest that both sequences were erupted from vent(s) on Mount Discovery and may be broadly the same age. ʻAʻā and likely pāhoehoe lava-fed deltas also occur at Helms Deep. Despite the ʻaʻā delta outcrop being significantly eroded, with its coeval capping subaerial ʻaʻā lavas entirely removed, paradoxically it yielded the youngest age in our study. Both outcrops at the locality appear to dip gently to the southeast, suggesting that they drape the Mason Spur succession and issued from vents on Mount Morning. Because all of the lava-fed delta outcrops examined issued from vents extrinsic to the Mason Spur volcano, they presumably represent discrete basanite magma batches unrelated to each other and to those that erupted at Mason Spur.

What caused the longevity of volcanism at Mason Spur?

Our study has highlighted how volcanism at Mason Spur extended between c. 13 Ma and present, which would be unusually long if they were associated with a single evolving polygenetic centre. However, Mason Spur is situated within the WARS close to the rift margin. It sits above relatively thick crust adjacent to the Transantarctic Mountain front, a major lithospheric discontinuity (Wright-Grassham 1987; Wilson et al. 2007; Martin et al. 2015, 2021b). It is also situated at the southern extension of the Terror Rift proposed by Horgan et al. (2005; Fig. 1) and on the southern margin of the Discovery accommodation zone. According to Granot and Dyment (2018), extension caused by rifting in the WARS ended at c. 11 Ma. Younger fault activity associated with the Terror Rift was considered to be related to intraplate deformation, perhaps associated with dextral strike-slip activity (Sauli et al. (2021). The younger faults are deep structures clearly imaged on seismic profiles (Sauli et al. 2021) and, along with a driver such as edge-driven mantle flow (Panter et al. 2018), would have facilitated the uprise of mafic magmas during extensional episodes (Rilling et al. 2009). While the history of the Discovery accommodation zone is unclear, the Terror Rift has experienced repeated extension since its initiation, continuing into the Pliocene and Pleistocene, and the rift may still be active today (Paulsen and Wilson 2009; Martin and Cooper 2010; Sauli et al. 2021). Both zones of structural weakness, and the presence of a translithospheric fault promoting edge-driven mantle flow (Faccenna et al. 2008, Panter et al. 2018; Panter and Martin, 2021), may be responsible for the eruption of mafic (mainly basanitic) magmas at Mason Spur after the initial burst of trachytic activity at 13–12 Ma. Thus, we envisage basanite magma being emplaced into thick, rift-marginal crust where it fractionated to yield the trachytes of unit MSP1 (Wright-Grassham, 1987). Later basanite magmas were smaller in volume and were linked to lesser extensional events. They traversed the crust via deep faults linked to the Terror Rift and the mafic compositions suggest that they probably did not stall in shallow crustal magma chambers. The magmatic longevity seen at Mason Spur is therefore a consequence of magma production within an evolving rift experiencing multiple episodes of extension over several million years.

What triggered the major caldera-forming eruption at Mason Spur (unit MSP1)?

Significant caldera eruptions, like that which occurred at Mason Spur, are associated with eruption rates at the middle to upper end of the range preserved in the rock record (Costa and Martí 2016; Giordano and Cas 2021). Some of the largest are related to felsic caldera eruptions, e.g., Oruanui, New Zealand (Wilson et al. 2006). The common occurrence of felsic batholiths in the rock record shows that accumulation of evolved magma in the upper crust is not unusual but the infrequency of significant felsic caldera eruptions compared with felsic batholith occurrences indicates that specific conditions must be met in order to trigger those eruptions (Jellinek and DePaolo 2003). Felsic caldera eruptions from large magma chambers typically occur in settings characterised by low rates of magma production (Jellinek and DePaolo 2003). Other factors may be important (e.g., far-field tectonic forces, magma crystal content, lateral magma transport, effective viscosity of wall rocks, thick continental crust, and deglaciation or ice cap retreat; Jellinek and DePaolo 2003; Costa and Martí 2016; Sulpizio and Massaro 2017). The eruptions also involve shallow (4–10 km) magma chambers and they occur in island arc, continental rift or extensional settings (Jellinek and DePaolo 2003; Costa et al. 2011; Gregg et al. 2015; Costa and Martí 2016). Rates of magma production in the WARS are roughly 10^{-7} km^3 year^{-1}, assuming a maximum volume of 10^6 km^3 erupted over 50 Ma (Behrendt et al. 1994; Rocchi et al. 2002). This overlaps with the range of magma production of other, similarly sized continental rifts (Panter 2021), e.g., the Basin and Range province (USA) at 10^{-5} to 10^{-7} km^3 year^{-1} (Crowe 1986). At these slow magma production rates, the relatively large magma chamber needed to feed the > 85 km^3 Mason Spur eruption would have required a long period of accumulation without eruption, probably 10^5 years or more (Jellinek and DePaolo 2003).

To trigger a significant caldera eruption requires (1) magmatic overpressure or (2) external forces, such as far-field stresses or foundering of the magma chamber roof (e.g., Wilson et al. 2006; Costa et al. 2011; Allan et al. 2012; de Silva and Gregg 2014; Gregg et al. 2015). The former involves a triggering pressure within the reservoir that exceeds the lithostatic confining pressure (Gregg et al. 2015). It may

occur during magma recharge leading to variation in buoyancy, crystal cargo or volatile content (Wark et al. 2007; Caricchi et al. 2014; Malfait et al. 2014). Gregg et al. (2015) calculated that a rheological threshold for an eruption is surpassed once the magma chamber volume exceeds around 100 km^3. The role of far-field stresses is often harder to determine given that the trigger may not be preserved in the rock record, something Allan et al. (2012) referred to as *the invisible hand*. In the following paragraphs, we outline the conditions relevant to Mason Spur unit MSP1 that may lead to a significant eruption, including our preferred hypothesis, without implicitly demonstrating causation.

The WARS is conventionally considered to have stalled at c. 26 Ma (DeMets and Merkouriev 2016; Sauli et al. 2021), which implies that there was no far-field stress driver. However, motion between West and East Antarctica may have continued until Middle Neogene time, c. 11 Ma (Granot and Dyment 2018). This includes accommodation of motion in the Terror Rift offshore of southern Victoria Land. The revised middle Neogene age of rifting coincides with the significant felsic caldera eruption at Mason Spur (MSP1) and a causal link is plausible.

Magmatism in the Mount Morning Volcanic Field is considered to have commenced by at least 25 Ma (Martin et al. 2021a, b). McMurdo Volcanic Group magmatism is generally thought to have anomalously heated the lithosphere both in Victoria Land and in the western Ross Sea (Berg et al. 1989; Wörner and Zipfel 1996; Martin et al. 2014; Shen et al. 2020; Wiens et al. 2021). Thus, the MSP1 ignimbrite eruptions at Mason Spur were preceded by more than 10 Ma of magmatism, during which the crust was thermally preconditioned (Jellinek and DePaolo 2003).

Deglaciation might be an additional factor (Jellinek et al. 2004; Geyer and Bindeman 2011; Nyland et al. 2013; Sulpizio and Massaro 2017). For example, a retreating ice body less than a kilometre thick may depressurize shallow magma systems, whilst larger ice masses may even influence melt generation down to mantle depths (Gudmundsson 1986; Sigmundsson et al. 2010). A potential contributing factor triggering the eruption of MSP1 at Mason Spur might thus be significant fluctuations in ice thickness during and immediately following the Middle Miocene Climate Transition, a period of significant climate instability (Halberstadt et al. 2021; Levy et al. 2021).

In summary, major conditions favorable for a significant felsic caldera eruption at Mason Spur involved (1) a rift setting (WARS/Terror Rift), and (2) motion between East and West Antarctica continuing to the middle Neogene. Additional factors that probably contributed include (3) a low rate of magma production, (4) thermal pre-conditioning of the lithosphere, and possibly (5) ice unloading. All of these circumstances may have acted in unison.

Comparison of Mason Spur with other volcanoes in the West Antarctic Rift System

As a result of this study, the Mason Spur volcanic complex is now one of the best described and dated centres in the WARS. The only comparable study is by Panter et al. (1994) for Mount Sidley (Marie Byrd Land). However, information is also available for a few other well-exposed centres such as Crary Mountains and Mount Murphy (Marie Byrd Land), and Minna Hook and Hallett Coast volcanoes (Victoria Land; LeMasurier et al. 1994; Wilch and McIntosh 2002; Smellie et al. 2011a; Smellie and Martin 2021; Smellie and Rocchi 2021; Wilch et al. 2021). None closely resembles Mason Spur. The principal distinguishing features of the Mason Spur volcanic complex are (1) abundant ignimbrites (unit MSP1 and top of unit MSP3); (2) conspicuous epiclastic rocks (mainly unit MSP3); (3) several tuff cones (MSP4 and MSP7); and (4) presence of lava domes (unit MSP8 and implicated in unit MSP3). Moreover, the volcanism at Mason Spur appears to have occurred intermittently and frequently over a period of c. 13 Myr, longer than any other WARS volcanic centre documented so far, apart from Mount Morning (Martin et al. 2021a; Wilch et al. 2021).

Lava domes are scarce in the WARS but are present on several of the large volcanoes in the Erebus Volcanic Province (Wright-Grassham 1987; Smellie and Martin 2021). Mount Sidley is principally a phonolite—trachyte volcano with a 1.5 Myr life span. It formed from the overlapping products of three major centers (Panter et al., 1994). Two of the centers experienced caldera collapses but they lack tephras ejected during the caldera-forming events. Ignimbrites are present on one centre and were probably erupted from a flank vent. They are volumetrically minor and the bulk of the erupted products are ʻaʻā lavas; one center also experienced a significant trachytic airfall eruption. The evolution of all the other WARS centers are alike, and they are dominated by effusion of mafic glaciovolcanic ʻaʻā lava-fed deltas (Smellie 2021). Apart from numerous small scoria cones and a few tuff cones, tephras are minor and epiclastic deposits are virtually absent (e.g., glacial diamicts at Mount Murphy; Wilch and McIntosh, 2002). Overlapping centers also occur at Crary Mountains and along the Hallett Coast, the latter linked to eruptions from major coast-parallel fissures (Wilch and McIntosh 2002; Smellie and Rocchi 2021; Wilch et al. 2021). Calderas are present at several of the Hallett Coast centres and elsewhere in the Erebus Volcanic Province but they lack associated caldera-related tephras. Ignimbrites are absent. Like Mason Spur, the lifetimes of the major edifice-building periods for volcanoes within the WARS are typically about 1–2 Myr. Much younger activity, sometimes separated by as much as 8 Myr, often occurred but is represented mainly by scoria cones (Wilch et al. 2021)

whereas tuff cones are a prominent feature of the Mason Spur volcanic complex.

Despite the abundance of large polygenetic volcanoes with prominent summit calderas within the WARS (Panter et al. 1994; Smellie and Martin 2021; Smellie and Rocchi 2021; Wilch et al. 2021), large volumes of ignimbrites are associated only with two poorly known volcanic centres in Victoria Land, at Deception Plateau and possibly Malta Plateau c. 600 km north north-east of Mason Spur (Smellie and Rocchi 2021). Only one volcano in the WARS, at Mount Waesche (Marie Byrd Land), is associated with caldera collapse-related deposits (Dunbar et al. 2021). The Mount Waesche caldera is small in comparison (c. 2 km diameter) and the inferred deposits form a widespread thin (few metres) drape of polymict breccia on the volcano slopes; ignimbrite deposits are absent. Ignimbrites associated with caldera collapses also characteristically contain abundant accessory and accidental clasts derived from deep within the volcano interior and underlying basement (e.g., Druitt 1985; Druitt and Bacon 1986; Allen and Cas 1998). These clasts are absent from MSP1. Caldera collapses in large volcanic systems like Mason Spur, which vented abundant ignimbrites, are normally associated with explosive eruptions and the formation of thick extra-caldera ignimbrite deposits, except in unusual circumstances (e.g., Hildreth and Fierstein 2000; Lipman and McIntosh 2008).

The absence of major ignimbrite deposits preserved elsewhere in the WARS may be due to a combination of factors: (1) insufficient exposure into the deep interiors of other volcanoes; this seems unlikely as a general explanation given the absence or scarcity of ignimbrites from those volcanoes that are deeply eroded (Minna Hook, Hallett Coast volcanoes, Mount Sidley, Mount Murphy and Crary Mountains); or (2) the evidence was removed by ice advection. Smellie (2021) proposed that tephra-producing eruptions, including any ignimbrites, that occur during glacial periods would deposit their tephras in the surrounding ice. Ice movement would carry the tephras to the ice margins and dump the deposits into the sea, thus leaving little or no terrestrial record. Given the history of prolonged glacials in Antarctica (Halberstadt et al. 2021; Levy et al. 2021), this seems the most likely explanation for the scarcity of pyroclastic rocks generally within the WARS.

Conclusions

Mason Spur is the remnant of a polygenetic volcanic complex in southern Victoria Land, part of the Mount Morning Volcanic Field in the Erebus Volcanic Province (McMurdo Volcanic Group). The deep interior of the complex is unusually well exposed due to the coastal location and the combined effects of focussed marine and glacial erosion. The outcrops have been divided into multiple stratigraphical units based on field relationships, the predominant lithofacies, and differences in isotopic age. Together they provide a rare and exceptionally detailed geological history involving eruptions over a particularly prolonged period (c. 13 Myr) within the intracontinental West Antarctic Rift System.

The oldest-exposed and most voluminous eruptive unit (MSP1) consists of indurated, deformed, massive trachytic ignimbrites together with pre- and post-caldera hypabyssal intrusions. The ignimbrites are undated but were probably erupted around c. 13 Ma (Middle Miocene). They were invaded by abundant hypabyssal intrusions, the oldest of which were pervasively brecciated during a major volcanotectonic event (i.e., that which formed the caldera). MSP1 is interpreted as a caldera fill and empirical calculations suggest that a minimum volume of c. 85 km^3 of volcanic products accumulated *within the caldera*. The caldera must have formed between 13 and 12.6 (possibly 12.9) Ma, the latter being an age obtained on the oldest fluidal-margined intrusion emplaced in the early post-caldera period. Unit MSP1 was profoundly eroded prior to and following the eruption of several younger units. A substantial palaeo-relief was created, possibly triggered by base-level readjustment due to uplift. Ravines hundreds of metres deep were cut and infilled by trachytic coarse mass flow deposits (MSP3). These are interbedded with sandstones representing multiple lahar and lahar runout deposits, and were probably sourced in gravitational collapses of one or more trachyte domes. Unit MSP3 also includes a thin unit of fresh white trachytic ignimbrites. It was succeeded, after further erosion, by effusion of thick basanite lava flows and additional mass flow deposits (MSP6). The intrusive activity represented within MSP1 lasted from 12.9 until 11.2 Ma. The intrusive magmas, which are mainly trachytic but include rare basanites and alkali basalts, probably fed multiple small centres, resulting in eruption of trachytic lava flows (MSP2) and a tuff cone (MSP4), together with basanitic lava flows (MSP5, MSP6) and pyroclastic cones (MSP7). This phase of activity lasted until about 10 Ma.

After a gap of c. 4 Myr, the final episode of trachyte eruption occurred at 6 Ma, creating a small trachyte lava dome and associated hot-emplaced block-and-ash-flow deposits (MSP8) followed by a prolonged pause in activity lasting 5 Myr. The most recent volcanic episode at Mason Spur is represented by two groups of small-volume basanitic magmas from several Pleistocene scoria cones (MSP9, MSP10), erupted at 0.94 and 0.37 Ma. The eruptions were dominantly Strombolian but early-formed lava flows in unit MSP9 were water-cooled, perhaps due to interaction with surface snow. Additionally, substantial basanitic lava-fed deltas of Pliocene and Pleistocene age were erupted from vents located on the

Mount Discovery and Mount Morning volcanoes, at 4.9 and 0.04 Ma, respectively. They are preserved as relicts flanking Mason Spur to the north, north-east and south-west.

The eruptive history and construction of the Mason Spur volcanic complex are dissimilar to any other volcanic center within the West Antarctic Rift System described so far. The most striking differences are the prolonged history of eruptions to form the present-day volcanic complex, and the abundance of ignimbrites in the main edifice-building phase. The differences are probably due to the location of the centre within a rift that was active prior to c. 11 Ma, which helped to trigger voluminous trachyte eruptions from a large crustal reservoir followed by a major caldera collapse. Subsequent eruptions were from multiple, small, mainly basanite centres linked to deep crustal faults created by residual intraplate deformation.

Supplementary Information The online version contains supplementary material available at https://doi.org/10.1007/s00445-022-01601-4.

Acknowledgements This study was inspired by the detailed field studies by Anne Wright-Grassham in the 1980s and we wish to publicly acknowledge her invaluable contribution to our understanding of the Mason Spur volcano and other volcanoes in the region. The present study was funded by the New Zealand Antarctic Institute (grant NZARI 2016-1-1 to Adam Martin). This work was also partly enabled by the New Zealand Government's Strategic Science Investment Fund support to GNS Science's Regional Geological Map Archive and Datafile (contract C05X1701) and supported by contract number ANT1801, with logistics support provided by Antarctica New Zealand. AM also gratefully acknowledges the support provided by the Geology Department, Otago University, for his fieldwork at Mason Spur in 2005. The authors are also grateful to our field assistants Matt Windsor and Benji Nicholson; Sean Mullally (Snow) & Andrew Hefford, pilots for Southern Lakes Helicopters; Peter McCarthy & Fiona Shanhun, Scott Base commanders and programme support supervisors; and Maddy Bellcroft, Scott Base operations scheduler (helicopter support). Samples collected by Anne Wright-Grassham and dated at the New Mexico Geochronology Research Laboratory were selected by Philip Kyle, whose help we are particularly grateful for. DR also thanks Bill McIntosh for his help supervising her Ar dating at the New Mexico Geochronology Research Laboratory. JS is grateful to Annika Burns (Leicester University) for making the numerous thin sections from often challenging samples that are also at the heart of this study, and for financial support provided by the Trans-Antarctic Association (UK). This paper benefitted from detailed reviews by Kurt Panter, Alan Cooper, Chris Waythomas, Philip Kyle, and Mark Stelten, and careful editorial handling by the editor, Michael Ort, for which the authors are grateful. The study is a contribution to the aims and objectives of AntVolc (SCAR Expert Group on Antarctic volcanism: https://scar.org/science/antvolc/home/). Any use of trade, firm, or product names is for descriptive purposes only and does not imply endorsement by the US Government.

References

Allan ASR, Wilson CJN, Millet M-A, Wysoczanski RJ (2012) The invisible hand: tectonic triggering and modulation of a rhyolitic supereruption. Geology 40:563–566

Allen SR, Cas RAF (1998) Lateral variations within coarse co-ignimbrite lithic breccias of the Kos Plateau Tuff, Greece. Bull Volcanol 59:356–377

Antoniades D, Giralt S, Geyer A et al (2018) The timing and widespread effects of the largest Holocene volcanic eruption in Antarctica. Nature Sci Reps 8:17279. https://doi.org/10.1038/s41598-018-35460-x

Behrendt JC, Blankenship DD, Finn CA, Bell RE, Sweeney RE, Hodge SM, Brozena JM (1994) CASERTZ aeromagnetic data reveal late Cenozoic flood basalts(?) in the West Antarctic rift system. Geology 22:527–530

Berg JH, Moscati RJ, Herz DL (1989) A petrologic geotherm from a continental rift in Antarctica. E Planet Sci Lett 93:98–108

Brand BD, Brož P (2015) Tuff cone. In: Hargitai H, Kereszturi Á (ed) Encyclopedia of Planetary Landforms, vol 2. Springer Science & Business Media LLC New York, pp 2197–2204, ISBN 978–1–4614–3133–6. https://doi.org/10.1007/978-1-4614-3134-3

Branney MJ, Kokelaar P (2002) Pyroclastic density currents and the sedimentation of ignimbrites. Geol Soci Lond Mem 27:143

Branquet Y, Cheilletz A, Giuliani G, Laumonier B, Blanco O (1999) Fluidized hydrothermal breccia in dilatant faults during thrusting: the Colombian emerald deposits. Geol Soc, Lond, Spec Publ 155:183–195

Caricchi L, Annen C, Blundy J, Simpson G, Pinel V (2014) Frequency and magnitude of volcanic eruptions controlled by magma injection and buoyancy. Nature Geosc 7:126–130

Costa A, Gottsmann J, Melnik O, Sparks RSJ (2011) A stress-controlled mechanism for the intensity of very large magnitude explosive eruptions. E Planet Sci Lett 310:161–166

Costa A, Martí J (2016) Stress field control during large caldera-forming eruptions. Front E Sci 4. https://doi.org/10.3389/feart.2016.00092

Crowe BM (1986) Volcanic hazard assessment for disposal of high-level radioactive waste. In Active tectonics: impact on society. The National Academy Press, Washington, DC, pp 247–260. https://doi.org/10.17226/624

de Silva SL, Gregg PM (2014) Thermomechanical feedbacks in magmatic systems: Implications for growth, longevity, and evolution of large caldera-forming magma reservoirs and their supereruptions. J Volcanol Geotherm Res 282:77–91

DeMets C, Merkouriev S (2016) High-resolution reconstructions of Pacific-North America plate motion: 20 Ma to present. Geophys J Intl 207:741–773

Di Vincenzo G, Bracciali L, Del Carlo P, Panter K, Rocchi S (2010) ^{40}Ar-^{39}Ar dating of volcanogenic products from the AND-2 core (ANDRILL Southern McMurdo Sound Project, Antarctica): correlations with the Erebus Volcanic Province and implications for the age model of the core. Bull Volcanol 72:487–505

Druitt TH (1985) Vent evolution and lag breccia formation during the Cape Riva eruption of Santorini, Greece. J Geol 93:439–454

Druitt TH, Bacon CR (1986) Lithic breccia and ignimbrite erupted during the collapse of Crater Lake Caldera, Oregon. J Volcanol Geotherm Res 29:1–32

Dunbar NW, Iverson NA, Smellie JL, McIntosh WC, Zimmerer MJ, Kyle PR (2021) Active volcanoes in Marie Byrd Land. Geol Soc, Lond, Mem 55:759–783

Faccenna C, Rossetti F, Becker TW, Danesi S, Morelli A (2008) Recent extension driven by mantle upwelling beneath the Admiralty Mountains (East Antarctica). Tectonics 7:TC4015. https://doi.org/10.1029/2007TC002197

Fielding RC (2018) Stratigraphic architecture of the Cenozoic succession in the McMurdo Sound region, Antarctica: An archive of polar palaeoenvironmental change in a failed rift setting. Sedimentology 65:1–61

Fielding CR, Henrys SA, Wilson TJ (2006) Rift history of the Western Victoria Land Basin: A new perspective based on integration of cores with seismic reflection data. In: Fütterer DK, Damaske D, Kleinschmidt G, Miller H, Tessensohn F (eds) Antarctica: Contribution to global earth sciences. Springer-Verlag, Berlin, pp 309–318

Fitzgerald P (2002) Tectonics and landscape evolution of the Antarctic plate since the breakup of Gondwana, with emphasis on the West Antarctic Rift System and the Transantarctic Mountains. Roy Soc NZ Bulletin 35:453–469

Geyer A (2021) Antarctic volcanism: active volcanism overview. Geol Soc, Lond, Mem 55:55–72

Geyer A, Bindeman I (2011) Glacial influence on caldera-forming eruptions. J Volcanol Geotherm Res 202:127–142

Giordano G, Cas RAF (2021) Classification of ignimbrites and their eruptions. E-Sci Rev 220:103697. https://doi.org/10.1016/j.earscirev.2021.103697

Granot R, Dyment J (2018) Late Cenozoic unification of East and West Antarctica. Nat Commun 9:3189. https://doi.org/10.1038/s41467-018-05270-w

Gregg PM, Grosfils EB, de Silva SL (2015) Catastrophic caldera-forming eruptions II: The subordinate role of magma buoyancy as an eruption trigger. J Volcanol Geotherm Res 305:100–113

Gudmundsson A (1986) Mechanical aspects of postglacial volcanism and tectonics of the Reykjanes Peninsula, southwest Iceland. J Geophys Res 91(B12):12711–12721

Halberstadt AR, Chorley H, Levy RH, Naish T, DeConto RM, Gasson E, Kowalewski DE (2021) CO_2 and tectonic controls on Antarctic climate and ice-sheet evolution in the mid-Miocene. E Planet Sci Lett 564:116908. https://doi.org/10.1016/j.epsl.2021.116908

Hildreth W, Fierstein J (2000) Katmai volcanic cluster and the great eruption of 1912. Geol Soc Am Bull 112:1594–1620

Horgan H, Naish T, Bannister S, Balfour N, Wilson G (2005) Seismic stratigraphy of the Plio-Pleistocene Ross Island flexural moat-fill: a prognosis for ANDRILL Program drilling beneath McMurdo Ice Shelf. Gl Pl Ch 45:83–97

Jellinek AM, DePaolo DJ (2003) A model for the origin of large silicic magma chambers: precursors of caldera-forming eruptions. Bull Volcanol 65:363–381

Jellinek AM, Manga M, Saar MO (2004) Did melting glaciers cause volcanic eruptions in eastern California? Probing the mechanics of dike formation. J Geophys Res 109(B9). https://doi.org/10.1029/2004JB002978

Jordan TA, Riley TR, Siddoway CS (2020) The geological history and evolution of West Antarctica. Nature Rev E Env 1:117–133

LeMasurier WE (2008) Neogene extension and basin deepening in the West Antarctic rift inferred from comparisons with the East African rift and other analogs. Geol 36:247–250

LeMasurier WE, Harwood DM, Rex DC (1994) Geology of Mount Murphy Volcano: an 8-m.y. history of interaction between a rift volcano and the West Antarctic ice sheet. Geol Soc Am Bull 106:265–280

Levy RH, Dolan AM, Escutia C et al (2021) Antarctic environmental change and ice sheet evolution through the Miocene to Pliocene – a perspective from the Ross Sea and George V to Wilkes Land Coasts. In: Florindo F, Siegert M, De Santis L, Naish T (eds) Antarctic Climate Evolution, 2nd edn. Elsevier, Amsterdam, pp 389–521

Lewis AR, Marchant DR, Ashworth AC, Hemming SR, Machlus ML (2007) Major middle Miocene global climate change: Evidence from East Antarctica and the Transantarctic Mountains. Geol Soc Am Bull 119:1449–1461

Lipman PW, McIntosh WC (2008) Eruptive and noneruptive calderas, northeastern San Juan Mountains, Colorado: Where did the ignimbrites come from? Geol Soc Am Bull 120:771–795

Le Maitre RW, Streckeisen A, Zanettin B, et al (2002) Igneous rocks. A classification and glossary of terms. Recommendations of the International Union of Geological Sciences Subcommission on the Systematics of Igneous Rocks. Cambridge University Press, Cambridge, pp 1–486

Malfait WJ, Seifert R, Petitgirard S, six authors, (2014) Supervolcano eruptions driven by melt buoyancy in large silicic magma chambers. Nature Geosc 7:122–125

Martí J, Geyer A, Aguirre-Diaz G (2013) Origin and evolution of the Deception Island caldera (South Shetland Islands, Antarctica). Bull Volcanol 75:1–18

Martin AP, Cooper AF (2010) Post 3.9 Ma fault activity within the West Antarctic rift system: onshore evidence from Gandalf Ridge, Mount Morning eruptive centre, southern Victoria Land. Antarctica Antarct Sci 22:513–521

Martin AP, Cooper AF, Dunlap WJ (2010) Geochronology of Mount Morning, Antarctica: two-phase evolution of a long-lived trachyte–basanite–phonolite eruptive center. Bull Volcanol 72:357–371

Martin AP, Cooper AF, Price RC (2013) Petrogenesis of Cenozoic, alkalic volcanic lineages at Mount Morning, West Antarctica and their entrained lithospheric mantle xenoliths: Lithospheric v. asthenospheric mantle sources. Geochim Cosmochim Acta 122:27–152

Martin AP, Price RC, Cooper AF (2014) Constraints on the composition, source and petrogenesis of plagioclase-bearing mantle peridotite. E-Sci Rev 138:89–101

Martin AP, Cooper AF, Price RC, Turnbull RE, Roberts NMW (2015) The petrology, geochronology and significance of Granite Harbour Intrusive Complex xenoliths and outcrop sampled in western McMurdo Sound, Southern Victoria Land, Antarctica. NZ J Geol Geophys 58:33–51

Martin AP, Smellie JL, Townsend CAF, DB, (2018) Formation of a spatter-rich pyroclastic density current deposit in a Neogene sequence of trachytic–mafic igneous rocks at Mason Spur, Erebus volcanic province. Antarctica Bull Volcanol 80:13. https://doi.org/10.1007/s00445-017-1188-7

Martin AP, Cooper AF, Price RC, Kyle PR, Gamble JA (2021a) Erebus Volcanic Province: petrology. Geol Soc, Lond, Mem 55:447–489

Martin AP, Cooper AF, Price RC, Doherty CL, Gamble JA (2021b) A review of mantle xenoliths in volcanic rocks from southern Victoria Land, Antarctica. Geol Soc, Lond, Mem 56. https://doi.org/10.1144/M56-2019-42

McKay R, Browne G, Carter L et al (2009) The stratigraphic signature of the late Cenozoic Antarctic Ice Sheets in the Ross Embayment. Geol Soc Am Bull 121:1537–1561

Miall AD (1977) A review of the braided-river depositional environment. E-Sci Rev 13:1–62

Miller SR, Fitzgerald PG, Baldwin SL (2010) Cenozoic range-front faulting and development of the Transantarctic Mountains near Cape Surprise, Antarctica: Thermochronologic and geomorphologic constraints. Tectonics 29:1–21

Nyland RE, Panter KS, Rocchi S, Di Vincenzo G, Del Carlo P, Tiepolo M, Field B, Gorsevski P (2013) Volcanic activity and its link to glaciation cycles: Single-grain age and geochemistry of Early to

Middle Miocene volcanic glass from ANDRILL AND-2A core, Antarctica. J Volcanol Geotherm Res 250:106–128
Olivetti V, Rossetti F, Balestrieri ML, Pace D, Cornamusini G, Talarico F (2018) Variability in uplift, exhumation and crustal deformation along the Transantarctic Mountains front in southern Victoria Land, Antarctica. Tectonophys 745:229–244
Panter KS (2021) Antarctic volcanism. Petrology & tectonomagmatic overview. Geol Soc, Lond, Mem 55:43–53
Panter KS, McIntosh WC, Smellie JL (1994) Volcanic history of Mount Sidley, a major alkaline volcano in Marie Byrd Land, Antarctica. Bull Volcanol 56:361–376
Panter KS, Castillo P, Krans S et al (2018) Melt origin across a rifted continental margin: a case for subduction-related metasomatic agents in the lithospheric source of alkaline basalt, northwest Ross Sea, Antarctica. J Petrol 59:517–558
Panter KS, Martin AP (2021) West Antarctic mantle deduced from mafic magmatism. Geol Soc, Lond, Mem 56. https://doi.org/10.1144/M56-2021-10
Panter KS, Talarico FM, Bassett K and 12 authors and the ANDRILL-SMS Science Team (2008) Petrologic and geochemical composition of the AND-2A core, ANDRILL Southern McMurdo Sound Project, Antarctica. Terra Antartica 15:147-192
Paulsen TS, Wilson TJ (2009) Structure and age of volcanic fissures on Mount Morning: a new constraint on Neogene to contemporary stress in the West Antarctic Rift, southern Victoria Land, Antarctica. Geol Soc Am Bull 121:1071–1088
Phillips WJ (1972) Hydraulic fracturing and mineralization. J Geol Soc, Lond 128:337–359
Pierson TC, Scott KM (1985) Downstream dilution of a lahar: transition from a debris flow to a hyperconcentrated streamflow. Water Res Res 21:1511–1524
Pierson TC, Waitt RB (1999a) Hydrologic consequences of hot-rock/snowpack interactions at Mount St. Helens volcano, Washington, 1982–84. Introduction. U S Geol Surv Prof Pap 1586:1–8
Pierson TC, Waitt RB (1999b) Dome-collapse rockslide and multiple sediment-water flows generated by a small explosive eruption on February 2–3, 1983. U S Geol Surv Prof Pap 1586:53–68
Pierson TC, Janda RJ, Thouret J-C, Borrero CA (1990) Perturbation and melting of snow and ice by the 13 November 1985 eruption of Nevado del Ruiz, Colombia, and consequent mobilization, flow and deposition of lahars. J Volcanol Geotherm Res 41:17–66
Pompilio M, Dunbar N, Gebhardt AC and 8 authors and the ANDRILL-MIS Science Team (2007) Petrology and geochemistry of the AND-1B Core, ANDRILL McMurdo Ice Shelf Project, Antarctica. Terra Antartica 14:255-288
Procter J, Zernack A, Mead S, Morgan M, Cronin S (2021) A review of lahars; past deposits, historic events and present-day simulations from Mt. Ruapehu and Mt. Taranaki, New Zealand. N Z Jl Geol Geophys 64:479–503
Rilling S, Mukasa S, Wilson T, Lawver L, Hall C (2009) New determinations of 40At/39Ar isotopic ages and flow volumes for Cenozoic volcanism in the Terror Rift, Ross Sea. Antarctica J Geophys Res 114:B12207. https://doi.org/10.1029/2009JB006303
Rocchi S, Armienti P, D'Orazio M, Tonarini S, Wijbrans JR, Di Vincenzo G (2002) Cenozoic magmatism in the western Ross Embayment: Role of mantle plume versus plate dynamics in the development of the West Antarctic Rift System. J Geophys Res 107:2195. https://doi.org/10.1029/2001jb000515
Rocchi S, LeMasurier WE, Di Vincenzo G (2006) Oligocene to Holocene erosion and glacial history in Marie Byrd Land, West Antarctica, inferred from exhumation of the Dorrel Rock intrusive complex and volcano morphologies. Geol Soc Am Bull 118:991–1005
Sauli C, Sorlien C, Busetti M, De Santis L, Geletti R, Wardell N, Luyendyk BP (2021) Neogene development if the Terror Rift, western Ross Sea, Antarctica. Geochem Geophys Geosyst 22.https://doi.org/10.1029/2020GC009076
Scott KM (1988) Origins, behavior, and sedimentology of lahars and lahar-runout flows in the Toutle-Cowlitz river system, Mount St. Helens, Washington. U S Geol Surv Prof Pap 1447-A:1–76
Scott KM, Vallance JW, Pringle PT (1995) Sedimentology, behavior, and hazards of debris flows at Mount Rainier, Washington. U S Geol Surv Prof Pap 1547:1–56
Shen W, Wiens DA, Lloyd AJ, Nyblade AA (2020) A geothermal heat flux map of Antarctica empirically constrained by seismic structure. Geophys Res Lett 47(14). https://doi.org/10.1029/2020GL086955.
Sigmundsson F, Pinel V, Lund B, Albino F, Pagli C, Geirsson H, Sturkell E (2010) Climate effects on volcanism: influence on magmatic systems of loading and unloading from ice mass variations, with examples from Iceland. Phil Trans Roy Soc A 368:2519–2534
Smellie JL (2021) Antarctic volcanism – volcanology and palaeoenvironmental overview. Geol Soc, Lond, Mem 55:19–42
Smellie JL, Martin AP (2021) Erebus Volcanic Province: volcanology. Geol Soc, Lond, Mem 55:415–446
Smellie JL, Rocchi S (2021) Northern Victoria Land. I. Volcanology. Geol Soc, Lond, Mem 55:347–381
Smellie JL, Rocchi S, Armienti P (2011a) Late Miocene volcanic sequences in northern Victoria Land, Antarctica: products of glaciovolcanic eruptions under different thermal regimes. Bull Volcanol 73:1–25
Smellie JL, Rocchi S, Gemelli M, Di Vincenzo G, Armienti P (2011b) Late Miocene East Antarctic ice sheet characteristics deduced from terrestrial glaciovolcanic sequences in northern Victoria Land, Antarctica. Palaeogeogr, Palaeoclimatol, Palaeoecol 307:129–149
Smellie JL, Wilch TI, Rocchi S (2013) 'A'ā lava-fed deltas: a new reference tool in paleoenvironmental studies. Geol 41:403–406
Smellie JL, Rocchi S, Johnson JS, Di Vincenzo G, Schaefer JM (2018) A tuff cone erupted under frozen-bed ice (northern Victoria Land, Antarctica): linking glaciovolcanic and cosmogenic nuclide data for ice sheet reconstructions. Bull Volcanol 80:12. https://doi.org/10.1007/s00445-017-1185-x
Smellie JL, Edwards BE (2016) Glaciovolcanism on Earth & Mars. Products, processes and palaeoenvironmental significance. Cambridge University Press. 483 pp
Sohn YK (1996) Hydrovolcanic processes forming basaltic tuff rings and cones on Cheju Island, Korea. Bull Volcanol 108:1199–1211
Sohn YK, Cronin SJ, Brenna M, Smith IEM, Nemeth K, White JDL, Murtagh RM, Jeon YM, Kwon CW (2012) Ilchulbong tuff cone, Jeju Island, Korea, revisited: a compound monogenetic volcano involving multiple magma pulses, shifting vents, and discrete eruptive phases. Geol Soc Am Bull 124:259–274
Sulpizio R, Massaro S (2017) Influence of stress field changes on eruption initiation and dynamics: a Review. Front E Sci 5. https://doi.org/10.3389/feart.2017.00018
Thouret J-C (1990) Effects of the November 13, 1985 eruption on the snow pack and ice cap of Nevado del Ruiz volcano, Colombia. J Volcanol Geotherm Res 41:177–201
Trabant DC, Waitt RB, Major JJ (1994) Disruption of Drift glacier and origin of floods during the 1989–1990 eruptions of Redoubt Volcano, Alaska. J Volcanol Geotherm Res 62:369–385
Wark DA, Hildreth W, Spear FS, Cherniak DJ, Watson EB (2007) Pre-eruption recharge of the Bishop magma system. Geology 35:235–238
White JDL, Houghton BF (2006) Primary Volcaniclastic Rocks Geol 34:677–680

White JDL, Ross PS (2011) Maar-diatreme volcanoes: a review. J Volcanol Geotherm Res 201:1–29

Wiens DA, Shen W, Lloyd AJ (2021) The seismic structure of the Antarctic upper mantle. Geol Soc, Lond, Mem 56, M56–2020–2018. https://doi.org/10.1144/M56-2020-18

Wilch TI, McIntosh WC (2002) Lithofacies analysis and $^{40}Ar/^{39}Ar$ geochronology of ice–volcano interactions at Mt. Murphy and the Crary Mountains, Marie Byrd Land, Antarctica. Geol Soc, Lond, Spec Publ 202:237–253

Wilch TI, McIntosh WC, Panter KS (2021) Marie Byrd Land and Ellsworth Land: volcanology. Geol Soc, Lond, Mem 55:515–576

Wilson TJ (1999) Cenozoic structural segmentation of the Transantarctic Mountains rift flank in southern Victoria Land. Global Planet Ch 23:105–127

Wilson CJN, Blake S, Charlier BLA, Sutton AN (2006) The 26·5 ka Oruanui eruption, Taupo volcano, New Zealand: development, characteristics and evacuation of a large rhyolitic magma body. J Petrol 47:35–69

Wilson G, Damaske D, Möller H-D, Tinto K, Jordan T (2007) The geological evolution of southern McMurdo Sound - new evidence from a high-resolution aeromagnetic survey. Geophys Jl Intl 170:93–100

Wilson GS, Levy RH, Naish TR et al (2012) Neogene tectonic and climatic evolution of the Western Ross Sea, Antarctica—Chronology of events from the AND-1B drill hole. Gl Pl Ch 96–97:189–203

Wörner G, Zipfel J (1996) A mantle P-T path for the Ross Sea Rift margin (Antarctica) derived from Ca-in-olivine zonation patterns in peridotite xenoliths of the Plio-Pleistocene Mt. Melbourne Volcanic Field Geol Jahrb B89:157–167

Wright AC, Kyle PR (1990) Mason Spur. Am Geophys Union, Antarct Res Ser 48:128–130

Wright-Grassham AC (1987) Volcanic geology, mineralogy, and petrogenesis of the discovery volcanic subprovince, southern Victoria Land, Antarctica. PhD thesis (geology). New Mexico Institute of Mining and Technology. 460 p [unpubl.]